Title
Toneless Bandpass Dynamic Element Matching

Author
Bergeron, Jarrah

Publication Date
2021

Peer reviewed|Thesis/dissertation

UNIVERSITY OF CALIFORNIA

Los Angeles

Toneless Bandpass Dynamic Element Matching

A thesis submitted in partial satisfaction of the requirements of the degree Master of Science in Electrical and Computer Engineering

by

Jarrah Gerald Bergeron

2021

ABSTRACT OF THE THESIS

Toneless Bandpass Dynamic Element Matching

by

Jarrah Gerald Bergeron

Master of Science in Electrical and Computer Engineering

University of California, Los Angeles, 2021

Professor Sudhakar Pamarti, Chair

Dynamic element matching (DEM) has been widely researched in the domain of digital-to-analog converters. Different architectures, noise shapes and ever higher order shaping have been devised. However, beyond first order, no schemes guarantee the absence of tones. Herein presents a band-pass shaping scheme that is provably toneless based on tree structured DEM. This scheme does incur a noise penalty and additional hardware. However, the former of which can be controlled and the later of which is only moderate.

The thesis of Jarrah Gerald Bergeron is approved.

Mau-Chung Frank Chan

Chih-Kong Ken Yang

Sudhakar Pamarti, Committee Chair

University of California, Los Angeles

2021

Table of Contents

List of Figures

List of Tables

1 Introduction

Communications, instrumentation, and radar applications commonly process high frequency, band-pass signals. Such signals may come from a variety of media but are often processed by heterodyne and direct conversion architectures. Such architectures process signals through a series of mixers, filters and local oscillators in one or multiple up-conversion or down-conversion stages. Direct radio frequency (RF) sampling does away with most of these analog components. Instead, signals are sampled at their original bands. As a result, much of the signal processing is brought into the digital domain which allows for simpler and more flexible systems. A key component to direct RF sampling is the high-speed digital-to-analog converter (DAC).

Direct RF sampling however imposes severe linearity constraints on the DAC. High-speed design necessitates small devices to reduce capacitance which is incongruent with device-to-device matching; shrinking devices accentuates statistical differences between them. If the DAC's devices are excessively mismatched, the sum contribution of those devices making up the output (be it current or voltage), will not track the DAC code. This leads to distortion in the intended signal. Distortion can manifest itself as spectral leakage, harmonics and poor reception quality, all of which are undesired. Effectively, the DAC does not behave linearly and techniques that suppress said distortion are desired. Dynamic element matching (DEM) is one such technique and is used in conjunction with certain DAC architectures.

A common DAC architecture is the thermometer DAC. This architecture is composed of many identical 1 bit DACs, called unit cells. In the simplest implementation, each unit cell can either contribute to the output or not. An example would be an array of CMOS current sources which are individually switched between the output or a dummy load. However, notice that for all DAC codes, except when all devices are on or off, the output can be taken from a plurality of unit cell combinations. A DAC code of 1 necessitates a single unit cell but any unit cell can be chosen. DEM takes advantage of this redundancy within thermometer

DACs. By carefully choosing DAC elements from one time step to the next, non-linearity arising from mismatched elements is mitigated. However, linearity does not come for free: noise and tones arise. Both effects are new and occur in addition to existing circuit noise.

The first effect of DEM, noise, can be remedied by being shaped. This shaping is analogous to how delta sigma ADCs and DACs suppress quantization error in low resolution DACs. In the case of direct RF sampling, RF signals are often band-pass in nature and shaping can suppress DEM noise in such a band. This is called band-pass DEM, or equivalently band-stop shaping. The later term emphasizes the suppression of in-band noise and is used synonymously in this text. With noise shaping, RF signals in said band are captured or constructed (for ADC and DACs, respectively) with higher fidelity. Tones, on the other hand, have been more difficult to remedy. They appear as extra signals, which in fact do not exist, thus compromising desired signal fidelity. The central contribution proposed herein is to eliminate tones in band-pass DEM.

Two band-pass DEM schemes are proposed: delta-sigma modulated (DSM) N-path DEM and reset-and-dither DEM. These two schemes eliminate tones while keeping the necessary noise shaping. Additionally, both schemes are arbitrarily tunable. A key benefit of the aforementioned direct RF sampling is in its flexibility and band-pass DEM should not limit which bands can be tuned. Both schemes are in keeping with such philosophy. In this text, DSM N-path is treated first. Its noise performance was poorer then the second proposal and thus only covered in modest detail. The dither-and-reset DEM is covered secondly, along with analysis of its tonal, noise performance and hardware impacts. Summaries of both techniques are covered at the end.

2 Dynamic Element Matching

As stated in the introduction, dynamic element matching (DEM) is a technique to linearise unit cell mismatches in thermometer DACs. Taking a thermometer current DAC, each unit cell is a current source where all current sources are ideally the same. These cells are turned on or off depending on the desired output current. The DAC code word represent this desired output current. For instance, if the code word is three, three unit cells are switched to the output. All the unit cells are ideally the same so hypothetically any set of three can be chosen. However, due to mismatch, this is not the case.

2.1 Early Work

Take the DAC shown in figure 1, it is composed of two unit current sources and generates one of three levels. Ideally, I_1 and I_2 are the same but they are not. As a result, the middle code word ('01') will not be precisely halfway between 0 and $I_1 + I_2$. Take the dotted waveform of figure 2. The DAC output, shown in the solid line, attempts to output this waveform but between t_1 and t_2, I_1 or I_2 can be selected. If I_1 is selected, the output will be below the ideal value (red). If I_2 is selected, the output is slightly above the ideal value (blue).

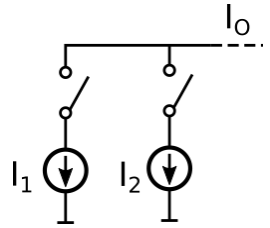

Figure 1: Three level DAC

The ideal value cannot be reached directly at any single point in time. However, the ideal value could be attained on average over time. One approach is to alternate between I_1 or I_2 whenever the middle level is requested. This was proposed in [1] and for the sake of this text will be called clocked averaging. The resulting waveform is shown in figure 3. Now between

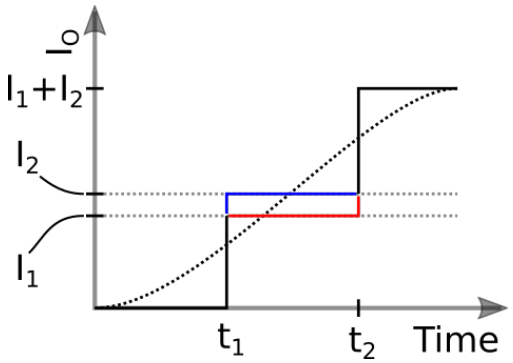

Figure 2: Waveform without DEM

t_1 and t_2, the waveform is on average $\frac{1}{2}(I_1 + I_2)$ and only limited by dynamic effects such as clock timing. Non-linearity is now reduced but the output contains an unwanted sinusoid proportional to the cell mismatch. Effectively, the power which would otherwise reside in the signal's harmonics now resides in a tone at half the sampling rate.

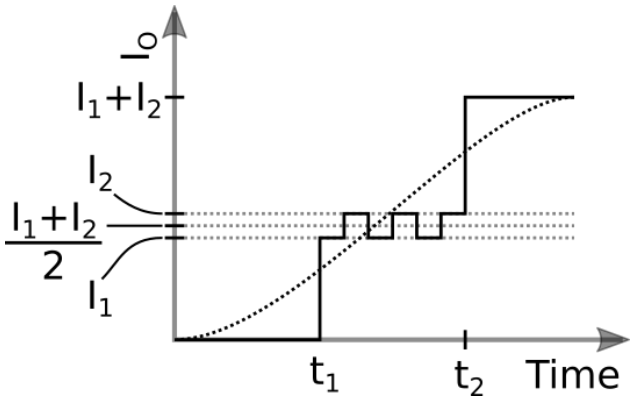

Figure 3: Waveform with DEM

Instead of simply alternating between unit cells, another approach would be to randomly choose unit cells, as first proposed in [2]. A possible waveform is shown in figure 4. As cells are chosen randomly, no extraneous tones are produced. Instead, the power which would otherwise reside in the signal's harmonics, or in a tone at half the sampling rate, now resides in white noise throughout the spectrum. Tones has now been traded for noise. This noise can be high-pass shaped as in data weighted averaging (DWA) in [3] if the intended signal is at low frequencies. However, DWA reintroduces tones. The trade-off between in-band noise

and tones is a theme in DEM.

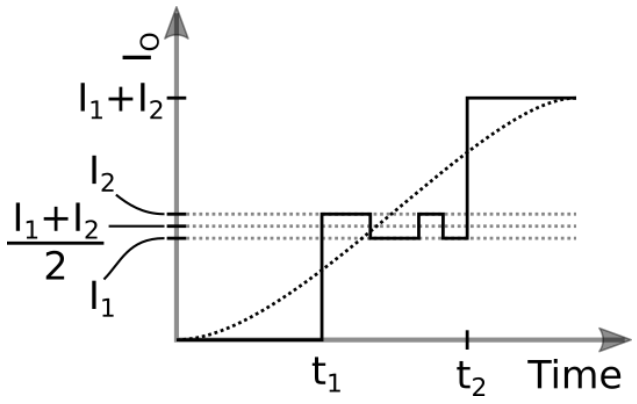

Figure 4: Waveform with DEM

2.2 Classes of DEM

Starting from this early work, two general classes of DEM architectures have since emerged: vector-based shaping and tree-structured shaping. Vector-based shaping was first introduced in [4] and can be thought of as an array of single bit delta sigma modulators with a shared quantizer, called a vector quantizer. The scheme is shown in figure 5. Double arrows denote vectors and each vector has the same size as the number of DAC unit cells. The DAC code word enters as $x[n]$ into the vector quantizer. The vector quantizer sorts $\bar{y}[n]$ and selects a $x[n]$ number of the largest $\bar{y}[n]$ values. The largest $\bar{y}[n]$ are denoted by corresponding ones in $\bar{x}[n]$, with the remainder being zero. For instance, if $\bar{y}[n_0] = [0.3, 0.2, 0.4]$ and $x[n_0] = 2$, $\bar{y}[n_0]$'s two largest entries are the first and last values; the output becomes $\bar{x}[n_0] = [1, 0, 1]$. The selection vector, $\bar{x}[n]$, in turn enables the appropriate unit cells.

The internal variable $\bar{y}[n]$ is computed from an array of feedback filters from $\bar{y}[n-1]$ and $\bar{x}[n-1]$. The original work featured a error feedback filter structure and is shown here as well. For high-pass shaping, $H(z) = 1 - z^{-1}$. A simple negation and delay is used within figure 5. However, this scheme offers shaping beyond first order as many transfer functions can be employed in $H(z)$. Another advantage is its low noise overhead but often has an

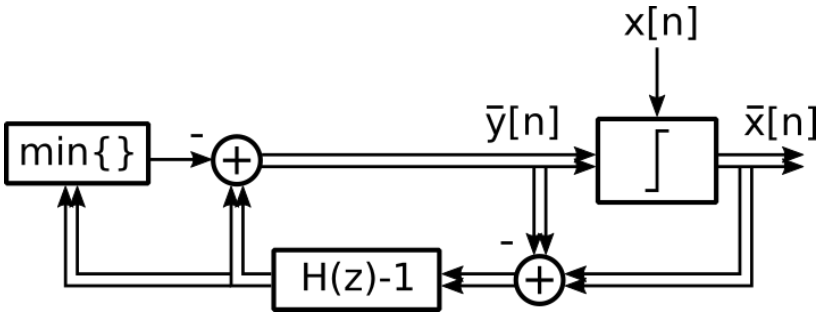

Figure 5: Vector-based shaping

expensive implementation due to the vector quantizer [5]. Sorting through many fixed-point numbers becomes prohibitive the larger the $\bar{y}[n]$ vector becomes.

The second architecture is tree-structured shaping and was introduced in [6]. As the name suggests, this architecture is in a form of a binary tree. The diagram of figure 6 shows its structure. The goal is to control many unit cells from a single code word. The multi-bit DAC code word, $x[n]$ enters the tree at the "trunk". Then, the tree repeatedly splits code words into pairs of progressively smaller bit-width codewords until they are single bits. The codewords reduce by one bit at each level. Switching blocks within each layer perform this function. At the tree's leaves, single bit codes ($x_1[n]$ through $x_8[n]$) control the unit cells. For the example 3 bit DAC shown, the first layer splits the 4 bit code $x[n]$, representing DAC levels 0 through 8, into two 3 bit codes $x_{3,1}[n]$ and $x_{3,2}[n]$. The process repeats till $x_1[n]$ through $x_8[n]$ are generated.

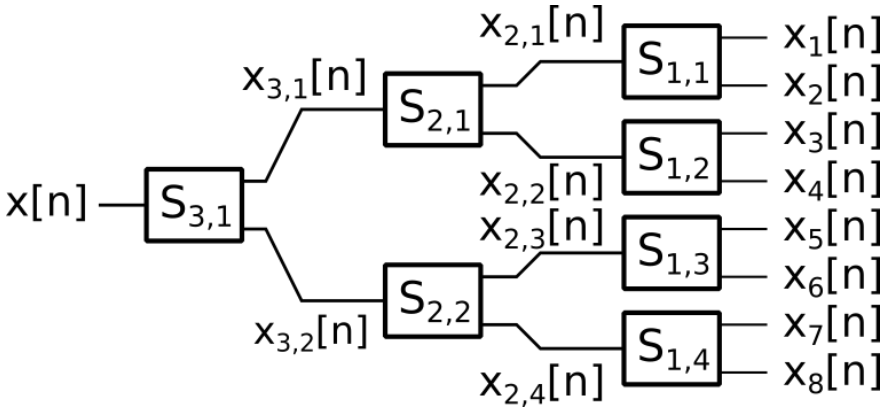

Figure 6: Tree structure DEM

Figure 7 shows the switching block structure. To reduce the codeword width, the main path splits and divides by two the incoming codeword. The codeword can be odd which would cause loss of information upon division as all $x_{k-1}[n]$ are integers. Therefore, before division, a sequence generator produces $s[n]$ which is added and subtracted from each branch to ensure a clean division. Its possible values are ± 1 if the codeword is odd or 0 if even. The sequence $O[n]$ indicates the parity of the incoming codeword. The sequence generator chooses ± 1 or 0 given the codeword parity. The advantage of this architecture is that noise shaping is fully determined by the weighted sum of power spectral densities (PSD) of all said sequence generators [7]. Hence, the DEM PSD is quite predictable. Also, tree-structured shaping is easier to implement with many elements [8]. The sequence generator is described next.

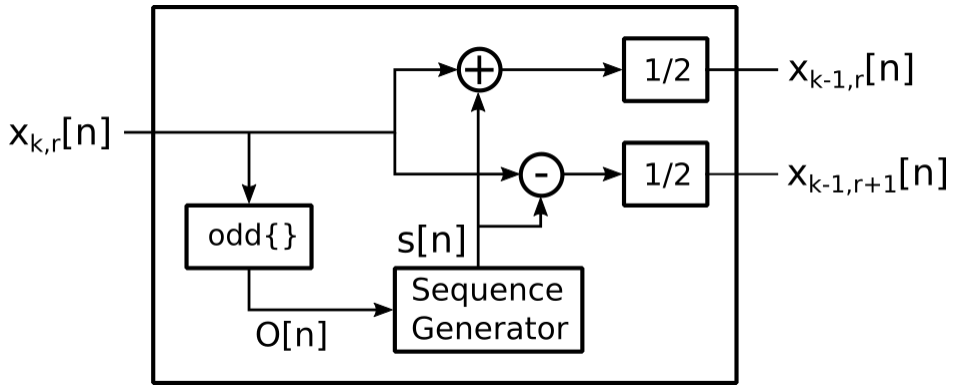

Figure 7: Switching block

The sequence generator lies at the heart of this scheme. To describe it, an example high-pass sequence generator is shown in figure 8. Starting at the quantizer, the parity indicator $O[n]$ indicates whether $s[n]$ should be ± 1 or 0; the quantizer quantizes $y[n] + d[n]$ only on odd parities of $x[n]$, otherwise it is zero. Negative feedback is created by feeding $-s[n]$ into an integrator. The integrator sums the output sequence $s[n]$ to generate $y[n]$. By negative feedback, it is ensured that the sum of $s[n]$ is bounded which guarantees a null in the PSD at zero frequency [7].

The dither, $d[n]$, ensures toneless behaviour and was subsequently proven to be toneless [9]. By adding an independent and identically distributed sequence, any repetition is broken. If the integrator ($y[n]$) is zero, dither causes a random ± 1 output to be made by the quantizer, independent of prior states.

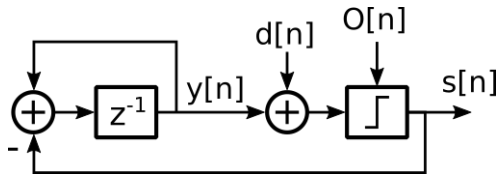

Figure 8: High-pass sequence generator

2.3 Toneless DEM

Many implementation and extensions have been reported from the two classes above. A few examples include higher order shaping [8] [10], band-pass DEM [11] [12] [13] [10] [14] and combined vector-based and tree-structured shaping [15]. However, toneless behaviour has not been guaranteed beyond first order low-pass DEM. Tones are not as common in such higher order schemes, but they do occur. This is demonstrated in the noise of figure 9 from a vector-based band-pass DEM shaper. Not only are these artefacts unwanted in many applications as outlined in the introduction, they are difficult to predict. Simulation of tones often require long Monte Carlo simulations and additional design margin [5]. This points to the need to develop other toneless DEM schemes, including flexible band-pass schemes for the direct RF sampling applications.

To extend toneless guarantees to bandpass DEM, both classes were examined. Between the two DEM classes, complete removal of tones has not been proven in first order vector based shaping. As such, the tree-structured architecture was developed further. The objective here will be to translate high-pass to band-stop noise shaping while preserving the absence of tones. Two schemes are presented.

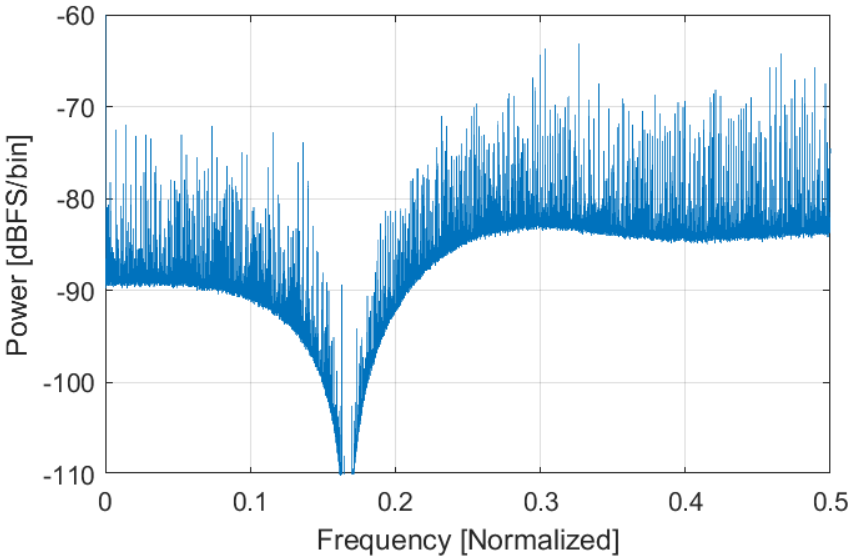

Figure 9: 2nd order vector-based DEM PSD

So called delta sigma modulator (DSM) N-path DEM, this scheme extends high-pass shaping to band-stop shaping using modulated N-path filters within tree structured DEM. N-path filters alone have been used within vector-based shaping and are straightforward to implement [13] [17]. Tuning and noise limitations are present, the former of which is remedied here with a DSM. The additional modulator toggles the number of paths to allow arbitrary band tuning. These features can be made while preserving toneless guarantees. Its noise performance was not satisfactory so this scheme is not emphasized in this work.

The second proposed scheme, so-called reset-and-dither DEM modifies previously reported on 2nd-order filter shaping [11] [14] [16]. This literature does not offer toneless guarantees. At best, hypothesises are provided in [16]. This work guarantees toneless operation when reset and dither is added. As such, tones are removed entirely, eliminating the design and system difficulties attributed to them. Noise performance and implementation considerations are also detailed within.

Closing out this section, it is instructive to define tonelessness. To be consistent with prior art in this domain [9], the same definition is adopted here. For a sequence $y[n]$ to

be toneless, the expected periodogram must be finitely bounded as its length approaches infinity.

$$\lim_{N\to\infty} E\{P_N(e^{j\omega})\} \leq K < \infty, \tag{1}$$

where the periodogram of $y[n]$ is

$$P_N(e^{j\omega}) = \frac{1}{N}\left|\sum_{n=0}^{N-1} y[n]e^{-j\omega n}\right|^2 \tag{2}$$

3 DSM N-path DEM

The first toneless band-pass scheme proposed is DSM N-path DEM. It is based off tree-structured shaping: the tree and the splitting blocks remain the same. Only the sequence generator is modified. As such, only the sequence generator will be described.

3.1 Proposed Structure

DSM N-path DEM modifies the sequence generators to an N-path filter approach. In a N-path structure, each path of a bank of identical filters (integrators in this case) is sequentially selected. Here, individual paths contain integrators which makes them indistinguishable from figure 8. However, with multiple paths, the prototype first order low-pass filter is transformed into a band-pass response. This approach has been used with vector-based shaping in [13] [14], [17] but not in a tree-structured architecture. Either way, the bands can only be placed on rational multiples of the sampling rate. Hence, a second adaptation is made such that band centres can be placed arbitrarily. As an apostle of delta sigma modulation, non-integer divisions can be attained by way of a delta sigma modulator (DSM).

The proposed structure, DSM n-path DEM, is shown in figure 10. As with N-path filters, a bank of integrators is placed inside the loop. The rest of the loop, including the quantizer, remains the same as a 1st order tree structured DEM. The quantizer outputs ± 1 or 0 if $x[n]$ is odd or even, respectively. The dither $d[n]$ causes a random decision to be taken when the selected path is zero. Switches selects a path at any given time but not all paths would be selected equally. A DSM coordinates whether to rotate through N or N-1 paths and a counter selects the required integrator from one clock cycle to the next. The DSM and counter can be shared amongst all the s-blocks in the tree. For this scheme, a simple first order DSM without dither was used. As for the number of paths (N), it is dictated by the lowest frequency to be tuned instead of the tuning resolution as with a traditional N-path implementation. For example, to tune to a center frequency of $1/3.5 = 0.2857$, 4

integrators would be needed instead of 7. Correspondingly, the path selection pattern would be 1,2,3,1,2,3,4... .

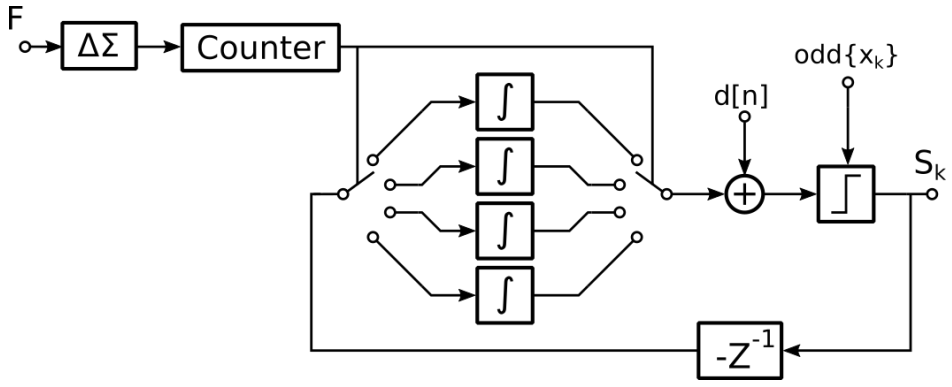

Figure 10: DSM N-path Sequence Generator

The path selection pattern is fully determined by the desired center frequency. As such given an input $O[n]$, this scheme is proved toneless as per theorem 1. If the $s[n]$ sequences of all s-blocks which make up the tree are toneless then the generated DEM noise will be toneless as per [7]. Evidently all s-blocks are identical so the entire DEM is toneless. Theorem 1 makes no statements on how path selection is performed so long it is predetermined; hence, many patterns can be used.

3.2 Simulation

Simulated DEM noise spectra and SNRs are shown in figure 11, with simulation conditions were as follows. The input waveform was a -6dBFS 4th order delta sigma modulated sinusoid. This sinusoid was 1 percent offset from each respective center frequency. The DAC constituted of 16 elements with 1 percent mismatch. Normalized center frequencies of 0.15, 0.3 and 0.45 are shown along with the non-DSM tree-structured shaper. The required number of paths were 7, 4 and 3, respectively instead of 10 paths without the DSM selection strategy. Bandpass shaping is indeed confirmed, along with the lack of tones. The noise minimum is band frequency dependent, generally following an inverse relationship. Because

of this reason, this scheme works best at lower center frequencies and OSRs even though no null is attained.

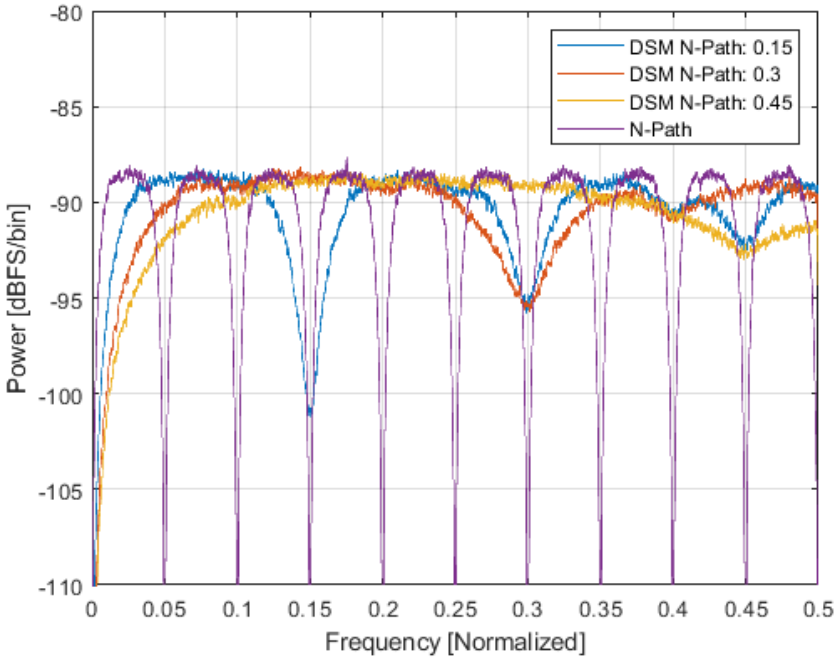

Figure 11: DSM n-Path DEM NSD at different f_c

Two other phenomena are of note. First, there is a persistent null at 0. The running sum is still bounded, albeit with multiple (but finite number of) integrators, and as a result a null at 0 will occur [7]. Secondly, shallower troughs are generated at band harmonics and their aliases, the clearest of which is the second and third harmonics of the 0.15 band located at 0.3 and 0.45, respectively.

Due the phenomena above and possibly others, DSM N-path does not shape as well as the second scheme in this work. Although, not covered yet, this is seen by comparing figures 11 and 26. As such, analysis will mostly end here. DSM N-path will be briefly mentioned in the implementation chapter. As a final note, a similar DSM selection scheme could be applied to the vector-based shaper. Such a strategy may yield lower noise but was not explored here. A vector based approach would however forego toneless guarantees and

implementation simplicity.

4 Reset-and-Dither DEM

The second toneless band-pass DEM scheme is presented here. First, the basic band-pass DEM scheme is described without ensuring the lack of tones. Then, two modifications are made. The first introduces a dither region which suppresses tones. The second adds periodic reset which eliminates tones entirely. Combining both modifications makes up the scheme proposed herein: reset-and-dither DEM.

4.1 Resonator Based DEM

To start, basic band-pass DEM is derived as follows. The high-pass shaping can be modified into band-stop shaping by modifying the integrator. To do so, the integrator's DC pole is moved. Therefore, the transfer function of an integrator, equation (3) becomes the transfer function (4). As this transfer function updates $y[n]$ with the fed-back values $s[n]$, the corresponding iterative function becomes equation (5). This equation is the function the sequence generator must implement. However, $y[n]$ is now complex and cannot be quantized directly as only a real $s[n]$ is desired. Proceeding logically, only the real portion of $y[n]$ is quantized and the sequence generator of figure 8 becomes figure 12.

$$H(z) = \frac{1}{1 - z^{-1}} \tag{3}$$

$$H(z) = \frac{1}{1 - z^{-1}e^{j\omega_c}} \tag{4}$$

$$y[n+1] = (y[n] - s[n])e^{-j\omega_c} \tag{5}$$

The structure in figure 12 can be redrawn into figure 13 where $y_r[n]$ and $y_i[n]$ denote the real and imaginary portions of $y[n]$. Effectively, the integrator has been turned into a

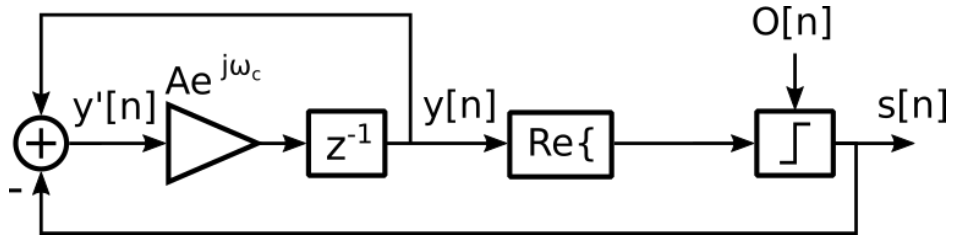

Figure 12: Bandpass DEM

resonator. Its structure is recognized to be the same as previous work [14][16]. It is also similar to [11] except here a state-space filter implementation is used instead of a direct form II implementation. The tonal performance of a direct from II implementation was not investigated but suspected to be similar. From either figures, a null in the PSD of $s[n]$ at ω_c is expected from equation (6), assuming the PSD of $y[n]$ is well behaved. An ill-behaved $y[n]$ with tones, may compromise this property or present tones in $s[n]$. Note that a complex implementation would simply add an imaginary $s[n]$ path from $y_i[n]$ with similar feedback. The question becomes how best dither be applied to avoid tones.

$$|S(e^{j\omega})|^2 = 2|Y(e^{j\omega})|^2(1 - \cos(\omega - \omega_c)) \tag{6}$$

4.2 Dither Region

It is not uncommon to add dither to break up tones in DSMs [5]. However, instead of considering dither as additive noise, dither can be viewed geometrically. To that end, the sequence generator's state plane is introduced.

To gain insight as to how the sequence generator behaves, its state can be tracked over time on a plane. Tracing its trajectory, a sort of "state diagram" or phase diagram forms. The concept is first shown for the first order high-pass sequence generator of figure 8. Figure 14 shows its states. For clarity, the integrator states are in blue. As there is only one state variable, the phase plane is simply the real line. At reset, the integrator is zero. At every

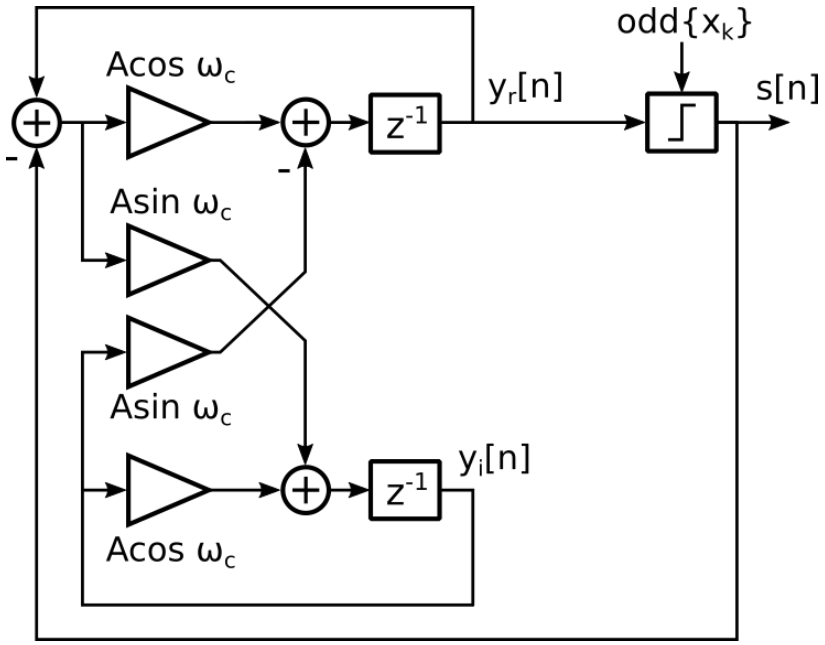

Figure 13: Basic 2nd Order band-pass DEM

even input, $s[n]$ is zero and the integrator stays at the same state. Once the first odd input arrives, denoted as a black 1 on the state diagram, the dither sets $s[n]$ to be ± 1 which is in turn subtracted from the integrator. This example will first assume the dither was 1; as a result, the integrator state will now move to the left to -1. At the next odd input, the integrator will still be at -1 and therefore $s[n]$ will be -1. The current $s[n]$ is subtracted from the integrator which returns the integrator to zero. If the dither was -1, the integrator state would instead have gone to +1 and come back to zero. As time passes, this process repeats. However, once the integrator goes back to zero, all previous information as to its state is lost.

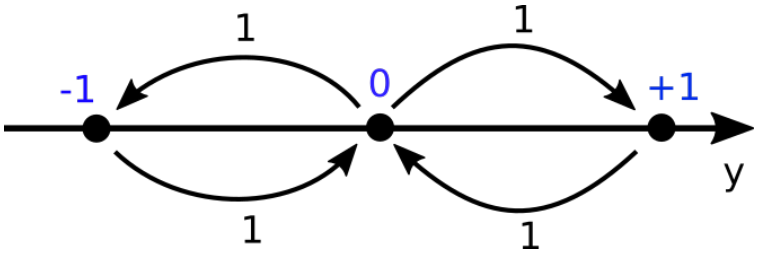

Figure 14: High-pass sequence generator state

With band-stop shaping, $y[n]$ is a complex variable so its phase diagram is a plane, in particular the complex plane. As well, there will be many more states. It is surmised that tones occurs if patterns are traced repeatedly on this plane. One in particular can be identified. If $\omega_c = \frac{2\pi}{6}$ and the $O[n]$ pattern "1,1,0,1,0,1..." is applied, the resonator will repeatedly trace the same pattern shown in figure 15. The $O[n]$ sequence was selected such that the first odd input places the resonator on a circle of magnitude 1 and odd inputs are fed whenever the resonator state is at $e^{j\pi/3}$ or $e^{j\pi 4/3}$. As such, once on the circle, the odd inputs will subtract ± 1 at those states but the resonator magnitude will stay the same and will always stay on the circle.

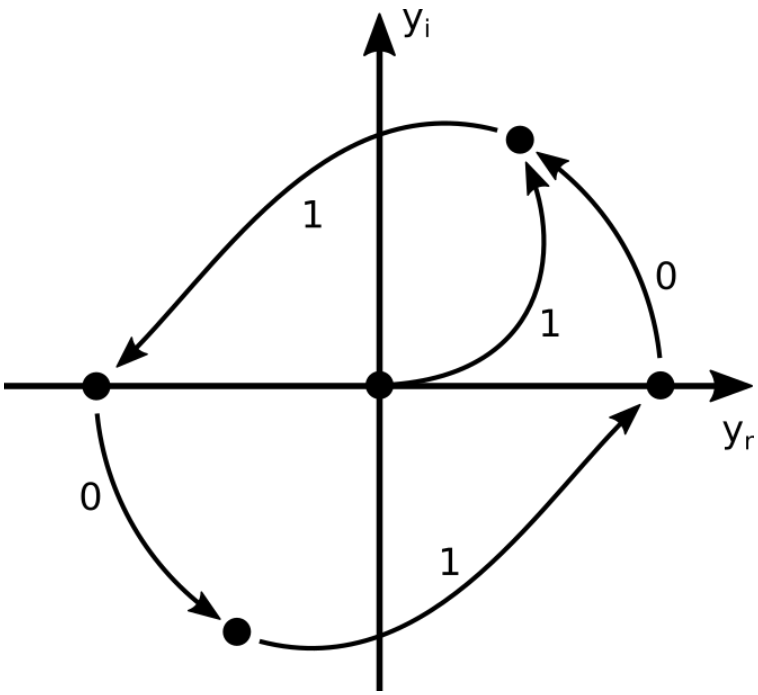

Figure 15: Problem Case

The resulting $s[n]$ sequence becomes "-1,+1,0,-1,0,+1..." and a tone occurs at $f_c = \frac{2\pi}{4}$. Many other center frequencies with appropriately constructed sequences will produce such patterns. Taking inspiration from first order shaping, a region can be added to break up patterns. The principle goes as follows.

When considering dither simply as added noise, depending on the resonator value, said

noise may not flip the quantizer frequently enough to mitigate tones. The goal is to guarantee dither will effect $s[n]$ at some finite point in time. Therefore, dither is only considered when it can effect the quantizer output ($s[n]$). The resonator values, $y[n]$, under such condition forms a region in the complex plane. This region is henceforth called the dither region. In the case of first order shaping, the integrator has values of 0 or ± 1 and unless zero, the dither has no effect. Therefore, dither can be viewed as many different regions which capture the origin but not ± 1. For instance, the dither region can be viewed as only the origin where dither is added at the resolution of the data type. Or perhaps, the dither region can be considered as much larger region instead. To extend this concept to band-stop shaping, this region must be thoroughly defined.

For band-stop shaping, the resonator may not attain zero with repeated odd codewords. This was illustrated in figure 15. Hence the dither region cannot simply be at the origin. It must be expanded to ensure $y[n]$ cannot be crossed over indefinitely at every odd codeword. One such region is a strip of width $|y_r| \leq \delta$ where $\delta > \frac{1}{2}$. This is shown as the grey box in figure 16. Here, the cycle first illustrated in figure 15 is broken. After point A, point B can be attained if $d[n] = 1$; however, B' can equally occur if the dither was negative, breaking up the potential cycle. The solid dots indicate $y[n]$ and the hollow dots, the intermediary result $y'[n]$ as denoted in figure 12.

Although shown only for a single example, if $\delta > \frac{1}{2}$, $y[n]$ will always end up inside the dither region within a finite number odd inputs, provided it is always of finite magnitude. Intuitively, the resonator does this: if $y[n]$ is outside the dither region, at every odd codeword the resonator magnitude will shrink and eventually spiral into the dither region. Once inside the dither region, a dither takes effect and a random ± 1 decision is made by the quantizer is made.

The modified sequence generator is illustrated in figure 17. The blue blocks are new. The magnitude comparator checks if $|y_r[n]| \leq 0.5$ and if so, ± 1 dither is fed to the quantizer.

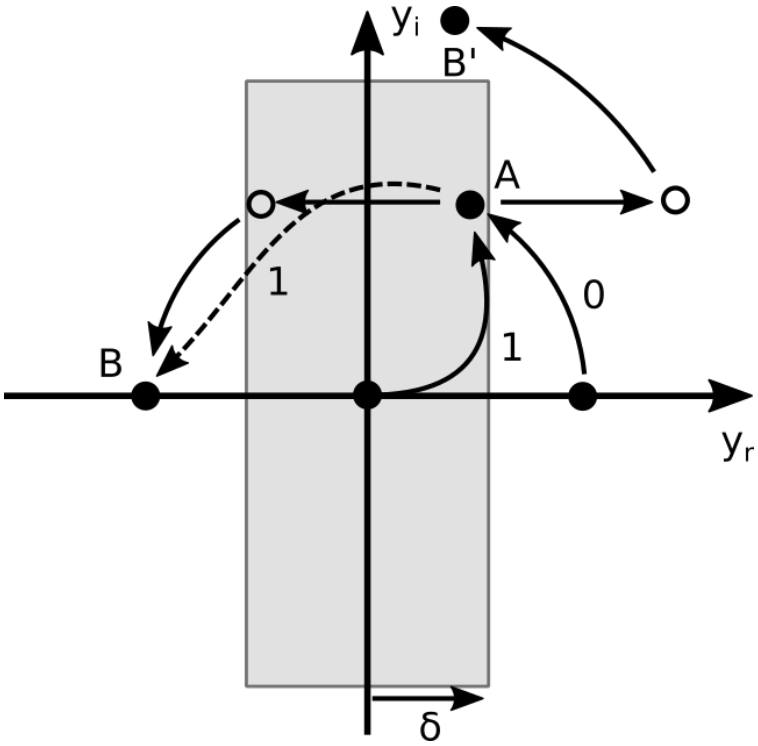

Figure 16: Dither region

If not, $y_r[n]$ is fed to the quantizer. A multiplexer switches the appropriate input to the quantizer. The sequence generator remains the same otherwise.

No proof is given as to the presence or absence of tones under this scheme. However, as will be discussed, there are few tones left with some sharp spectral peaking present. The sharp spectral peaking may or may not be indicative of tones and if of concern, can be fully resolved with a second technique which follows.

4.3 Resonator Reset

Another attribute of tone-free high pass shaping is that the integrator returns to zero on a regular basis with odd code words. Each time the integrator is zero, all information regarding prior states is lost. Combined with dither, the $s[n]$ sequence can then be split into uncorrelated symbols [9]. Effectively, the autocorrelation of $y[n]$ cannot extend beyond the next odd codeword and ensures the generated sequence has a finite PSD everywhere. In

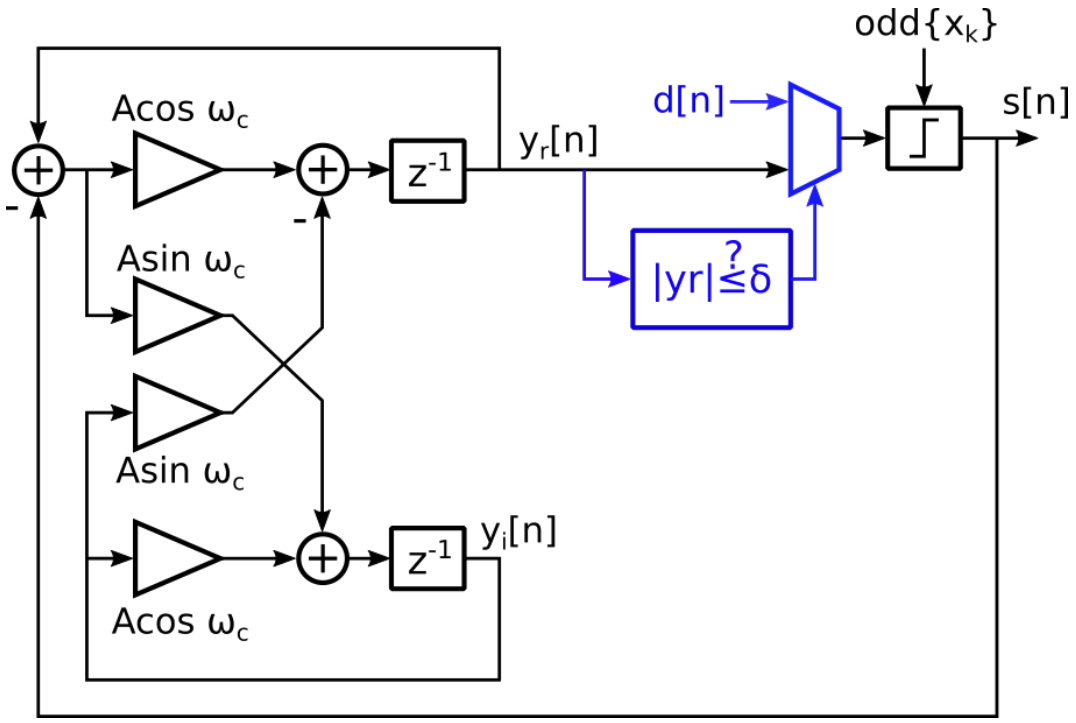

Figure 17: First modification: dither region

the band-stop shaping, expanding the dither region never fully ends $y[n]$'s autocorrelation. Therefore, ensuring a $y[n]$ of zero can be imposed through additional means.

This insight leads to the second modification. Simply be resetting the resonator at a regular interval will ensure $y[n]$ is zero regularly. The dither region is still present. Once a reset occurs, the dither will cause a random ± 1 decision in $s[n]$. Resets cannot occur too often either. In the extreme, if the resonator is reset at every time step, the autocorrelation does not extend beyond a zero offset and white noise results. Even if the resonator is reset at every other time step, only high-pass or low-pass shaping can be achieved. Effectively, the resonator at best acts like a two tap FIR filter. As such, the reset interval, denoted N_r, must be chosen accordingly.

The second modification is shown in red in figure 18. A counter tracks the time since the last reset. Once it times out, the resonator is cleared by switching in zeros. In the diagram, two multiplexers perform the switching but in an implementation, the flip-flops would simply

be cleared. With both modifications, the reset-and-dither scheme is complete. Analysis of the reset-and-dither DEM follows.

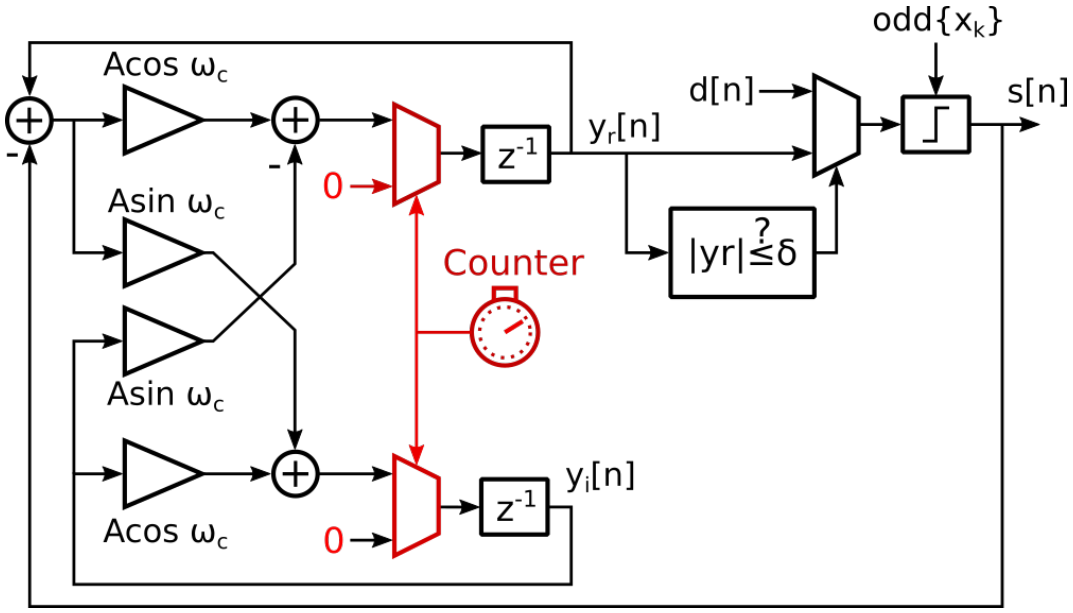

Figure 18: Reset-and-dither DEM with the second modification in red

First though, a statement regarding the absence of tones can be made as per the toneless definition of equations (1) and (2). Given an input sequence (and therefore $O[n]$) and a finite N_r, the sequence generator illustrated in figure 18 is toneless. The appendix provides the supporting theoretical foundation. Theorem 2 indicates the marginal PMFs of the real and imaginary portions of $Y[n]$ (capitalized to indicate a random variable) are symmetric about zero. This property is ensured by the symmetry of the iterative function and the dither. As such, for every resonator value, there is an equally likely resonator value of opposite sign which leads to an expectation of 0 as per lemma 1. From this fact, it is confirmed in theorem 3 that the autocorrelation of $y[n]$ cannot extend beyond a reset. The absence of tones is proven by the convergence of its periodogram which is indeed the case from theorem 4. If the resonator is always reset at multiples of N_r, the expected periodogram is at most N_r. This completes the behaviour of a single sequence generator.

The single sequence generator's spectral properties can be extended to the entire DEM

tree. From [7], the DAC output DEM noise is simply a linear combination of sequences $s_{k,r}[n]$. This combination is dependent of individual cell mismatches but the overall PSD properties are conserved. Certain subtleties do require addressing which relate to the theorem's conditioning on $O[n]$ and its independence from $d[n]$.

The first subtlety pertains to the construction of the DEM tree. As noted in [18], $d[n]$ can be shared amongst switching blocks of the same layer (at the possible expense of noise) but not between layers. If dither were shared between layers, $O[n]$ would be highly dependent on $d[n]$. Simply by employing separate $d[n]$ can this situation is avoided. The second subtlety arises once the DAC is integrated within a system. Feedback from the DAC output to its input, such as in $\Delta\Sigma$ ADCs, may introduce dither-to-input dependency. Fortunately, this is a rare occurrence in a realistic system with dynamic waveforms and multi-level DACs. Note that by themselves, $\Delta\Sigma$ DACs would not have this issue as feedback is not present.

In general, the theorems depend on the statistical properties of $y[n]$ and $s[n]$ being conditioned on the input parity $O[n]$, any sequence $O[n]$ but a given sequence none-the-less. Therefore, tones can occur if the current $O[n]$ is dependent on past non-zero $s[n]$ (and by extension, the dither $d[n]$). This requirement is implied in high-pass shaping as well. In [18], a requirement for uncorrelated symbols is that dither be independent of $O[n]$. However, this implies a lack of connection in both directions. Not only must dither be generated separately from $O[n]$ but $O[n]$ must not depend on past dither (and by extension, $s[n]$). Otherwise, inputs can be fabricated to break this independence.

An example input with high-pass shaping follows. An odd input is fed and the output is examined. If $s[n_0] = 1$ (or equivalently $d[n_0]$), an odd input is fed; otherwise, an even input is fed. At the third position, if $s[n_0] = 1$, an even input is fed; otherwise, an even input is fed. The process is repeated indefinitely with a period of three. These fabricated symbols are shown in (7) and (8). Starting from $n = 1$, every third output becomes -1 and from $n = 2$, every third output becomes 1. Hence, an inter-symbol correlation is created through

$O[n]$ and a tone is confirmed at $\frac{1}{3}$ Hz in the PSD of figure 19.

$$\begin{array}{c} d[n_0] \\ \downarrow \\ s[n] = \cdots, 1, -1, 0, \cdots \text{if } d[n_0] = 1 \\ \uparrow \\ -d[n_0] \end{array} \tag{7}$$

$$\begin{array}{c} d[n_0] \\ \downarrow \\ s[n] = \cdots, -1, 0, 1, \cdots \text{if } d[n_0] = -1 \\ \uparrow \\ -d[n_0] \end{array} \tag{8}$$

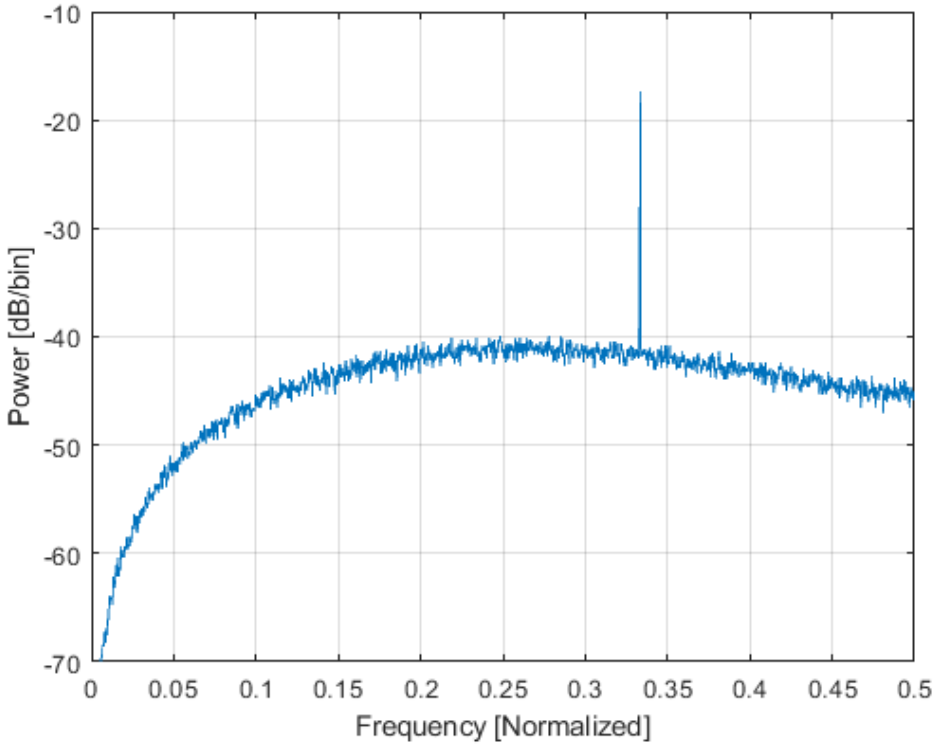

Figure 19: Sequence $s[n]$ dependent input PSD

5 Tonal Performance

Two tone mitigation strategies were covered: dither region and reset-and-dither. In this section, tonal performance is compared. First, tones from the individual sequence generators are analysed; problem sequences can be more easily identified in this situation. Tones at this stage would be indicative of tones from the entire tree but they may or may not be as severe. Tonal behaviour in a full tree is treated as well.

5.1 Sequence Generators

The overall tonal performance of the sequence generators are evaluated for various inputs $O[n]$. Considered inputs include square wave and $\Delta\Sigma$ modulator (DSM) waveforms. The analysis proceeds by finding the worst case inputs and DEM conditions under which tones are produced to gauge the robustness of each scheme. Other unwanted artefacts such as sharp PSDs are noted as well. The PSD $s[n]$ are plotted and not the outputs of the splitting block. As such, no features of the input waveform should be visible, including input tones. Typical plots are shown first followed by areas of concern. DEM parameters, whichever apply, are shown table 1. Frequencies are normalized where the sampling frequency is defined as 1. The DEM center frequency, f_c, of 0.21 in table 1 was chosen to present typical performance. Also, the dither region was set to $\delta = 0.501$ such that it is only slightly larger than $\frac{1}{2}$. Settings are modified as needed to highlight problem areas.

Parameter	Value
f_c	0.21
Reset Interval	128
Dither Region δ	0.501

Table 1: DEM parameters

5.1.1 Typical Behaviour

Both square waves and a DSM modulated sinusoid are considered for sequence generator typical performance. Square waves come about from periodic waveforms: periodic even and odd code words can create said square waves. As periodic waveforms appear often, square waves are considered. For the typical plot, input square wave of frequency 0.18 is applied near the DEM band center. The corresponding DEM NSD is shown in figure 20. Other than square waves, DSM waveforms are commonly encountered as well. For these simulations, the waveforms were assumed to be generated from a multibit modulator and only the least significant bit (LSb) was applied. This corresponds to the same condition as the first splitting block is placed in in the tree. The DSM properties are shown in table 21 and is also centred on a frequency of 0.18. The resulting DEM PSD is demonstrated in figure 21.

Parameter	Value
f_c	0.21
Backoff [dBFS]	-6
NTF	4th order band-pass

Table 2: DSM parameters

First, general comments are made in regards to tonal performance. For square wave inputs, tones are often produced if no dither region or reset-and-dither is applied. Shown in blue of figure 20, tones are clearly seen and are unwanted. However, both the dither region and the reset-and-dither DEM significantly improve tonal performance. The yellow and orange curves demonstrative this.

For DSM sinusoidal inputs, tones are much less frequent. This is likely due to the randomness inherent in the waveform. Figure 21 shows no sign of tones even without dither. However, tones or sharp spectral peaking are not unusual and can occur at various f_c of which there is no immediately discernible pattern. One example is demonstrated in figure 22 where the band center is near 1/6. The blue curve shows sharp peaks. It is not certain if these structures are tones. Randomness in the incoming waveform may perturb the sequence

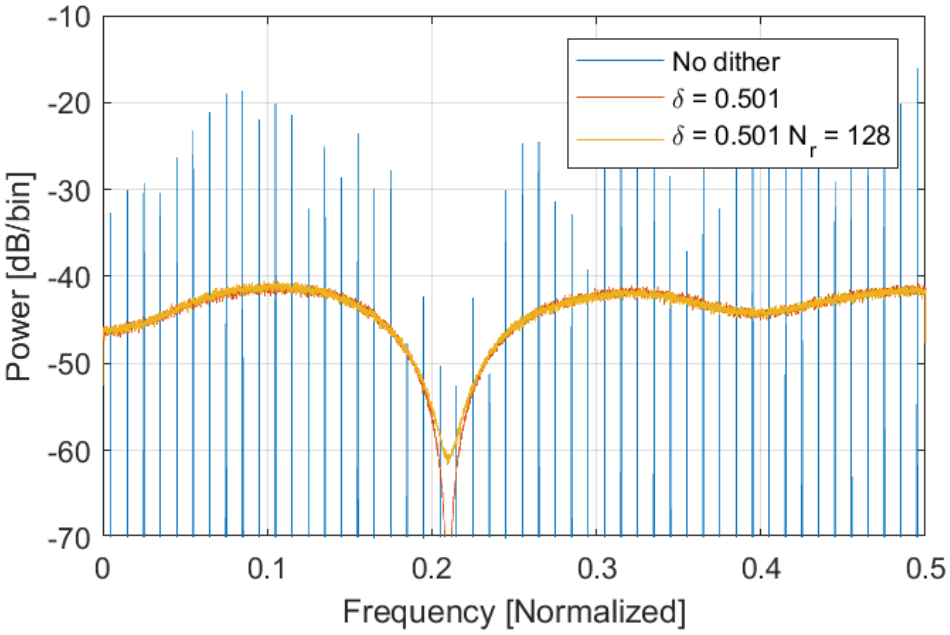

Figure 20: Typical DEM NSD with square wave input

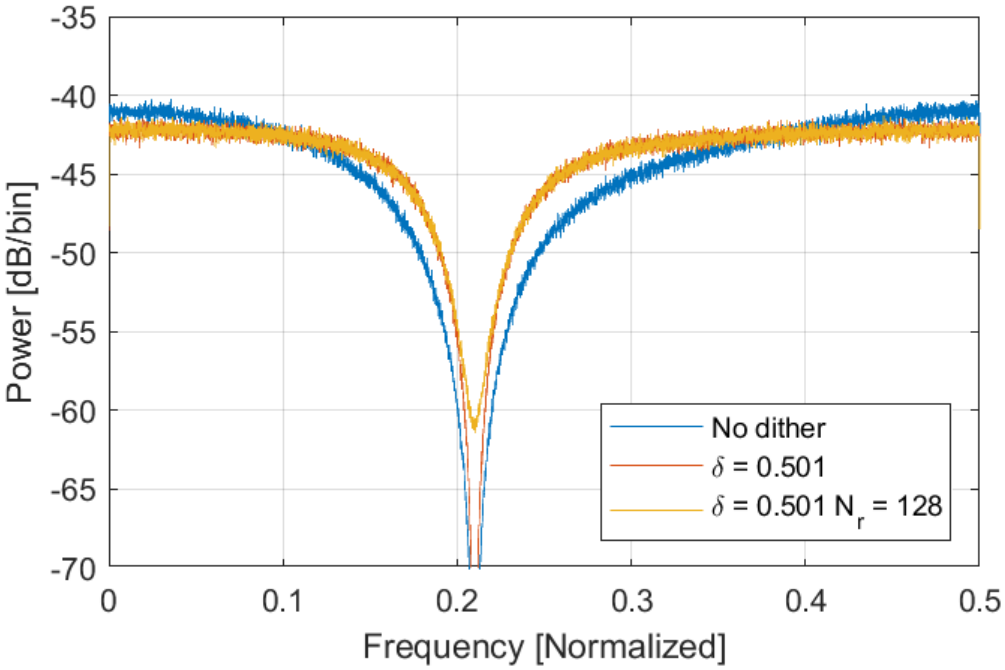

Figure 21: Typical DEM NSD with DSM sinusoid input

generators enough to move what would otherwise be tones and show up as peaks instead. However these peaks are generated, they are clearly unwanted. Both the dither region and reset-and-dither strongly suppress the aforementioned spectral peaks. These spectra confirm the need for tonal mitigation strategies. However, not all spectral concerns are mitigated. A few curiosities are covered next for both the dither region and reset-and-dither DEM.

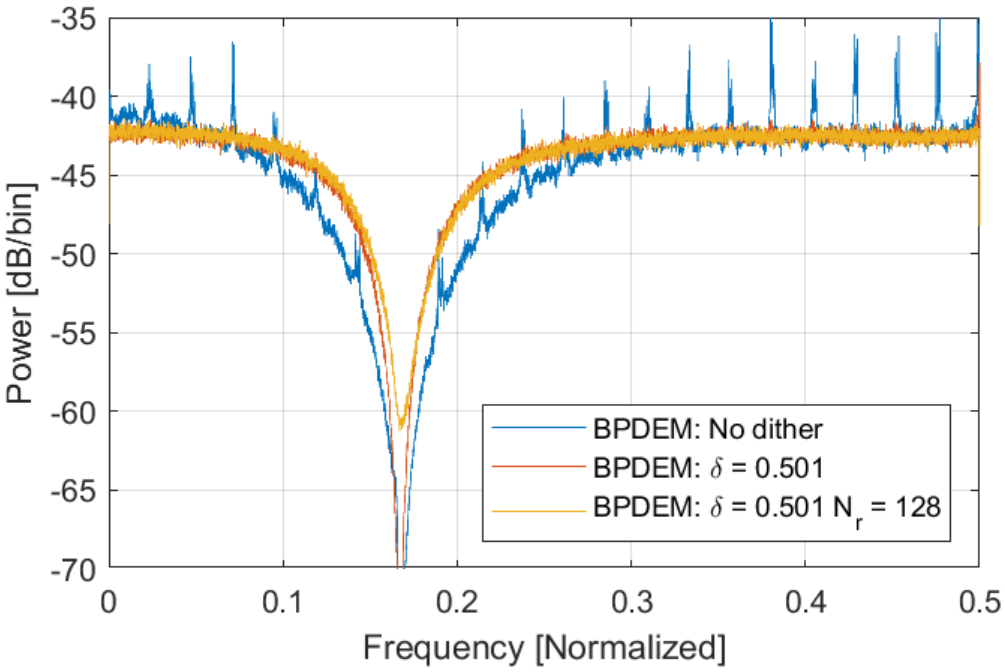

Figure 22: DEM NSD with problematic DSM sinusoid input

5.1.2 Dither Region

As demonstrated in the previous section, the addition of a dither region substantially cuts down on tones. However, problematic sequences still do arise. The primary area of concern is around $f_c = \frac{1}{12}$. Constant inputs and square waves of $f = \frac{1}{2}$ tend to produce sharp spectral peaking; the later case is shown in the blue curve of figure 23. The feature is not strictly confirmed to be a tone but closely resembles one. It should be noted that in general such peaking can appear elsewhere other than $\frac{1}{4}$, including near f_c.

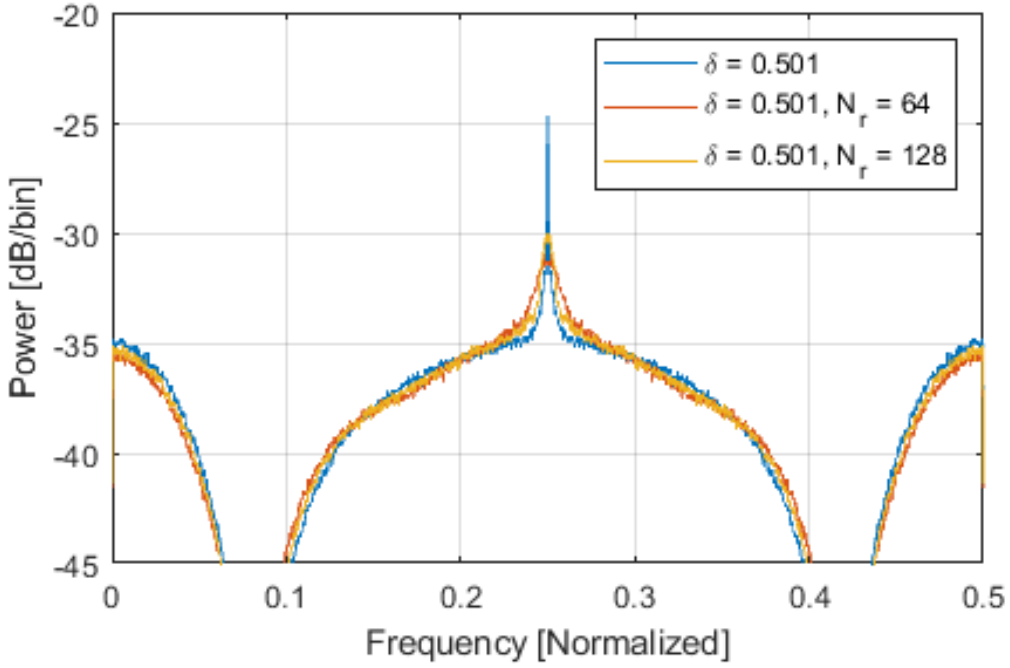

Figure 23: DEM NSD with problem square wave

With coefficient quantization, more center frequencies become of concern. They include $f_c = \frac{1}{6a}$ and $\frac{1}{2} - \frac{1}{6a}$ (where a is an integer greater than 1) when combined with an input waveform containing significant frequency content at $\frac{1}{6}f_c$. Quantization modifies the resonator gain (A) and the closer A is to 1, the worst the peaking gets. This tone-like behaviour can show up with DSM sinusoid inputs but they are rare. If the aforementioned behaviour is not of concern, solely a dither region can be applied. Otherwise, reset-and-dither DEM can be used

5.1.3 Reset-and-dither DEM

With resonator resets, no discernible tonal behaviour occurs, confirming theorem 4. In general, this scheme does not entirely produce the desired shaping; spectral peaking does occur, albeit not as sharp. Reset-and-dither DEM is plotted at two different N_r in figure 23. Zooming in, it is much clearer from figure 24 that the peak spreads out as N_r decreases.

Resetting and dithering occur more often so it is intuitively logical that this trend is observed. To characterize it, a metric of excess noise is defined: the height of a spectral peak versus if none where present. Its relationship with N_r is plotted through three cases in figure 25. Each case corresponds to different f_c and input waveform. The worse offenders sharpen at 3 dB per doubling of N_r.

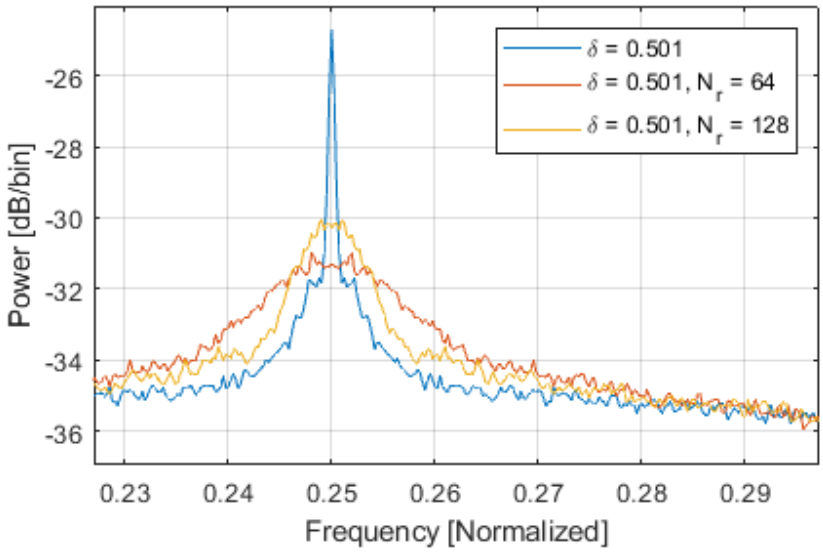

Figure 24: DEM NSD with problem square wave, zoomed in

Such behaviour is not unexpected. If a sinusoid where to develop within the resonator, upon reset, its opposite waveform could equally occur due to the symmetry in $Y[n]$'s PMF (as per theorem 2). Such a waveform is recognized to be a bipolar non-return-to-zero waveform, as common in communications theory, but modulated at said tone frequency. Assuming a magnitude of one, the PSD of such waveform follows the sinc relationship of equation (9). The peak PSD is indeed proportional to N_r from the 6 dB per octave shown in figure 25. As for the 3dB bandwidth, it approximately decreases inversely to N_r, as shown from the orange to the yellow curve of figure 24. Additionally, the side-lobes predicted in equation (9) can be seen if peaking is especially severe.

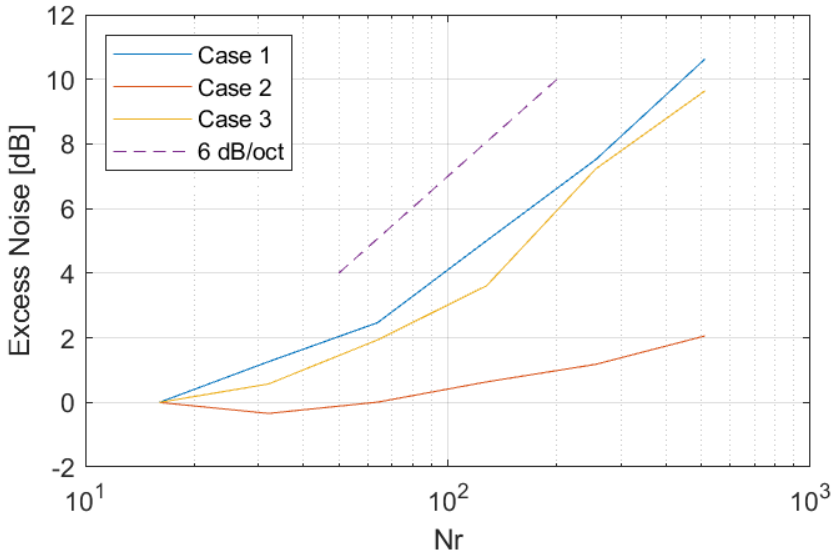

Figure 25: Peaking versus reset period

$$S\{f\} = N_r \frac{\sin(\pi N_r (f - f_c))^2}{(\pi N_r (f - f_c))^2} \tag{9}$$

5.2 Tree Structure

The tonal behaviour of a full DEM tree must be established as well. A typical DEM PSD of a 16 unit DAC is shown in figure 26. The PSDs of the presented schemes are very similar to that of individual sequence generators of figure 21. In fact, tonal performance of individual sequence generators readily apply to multi-level DEM. Regions around $f_c = \frac{1}{6a}$ and $\frac{1}{2} - \frac{1}{6a}$ are still concerning, especially for a = 1 and with coefficient quantization. As compared to individual sequences, tones and spectral peaking can be more or less severe in the full tree.

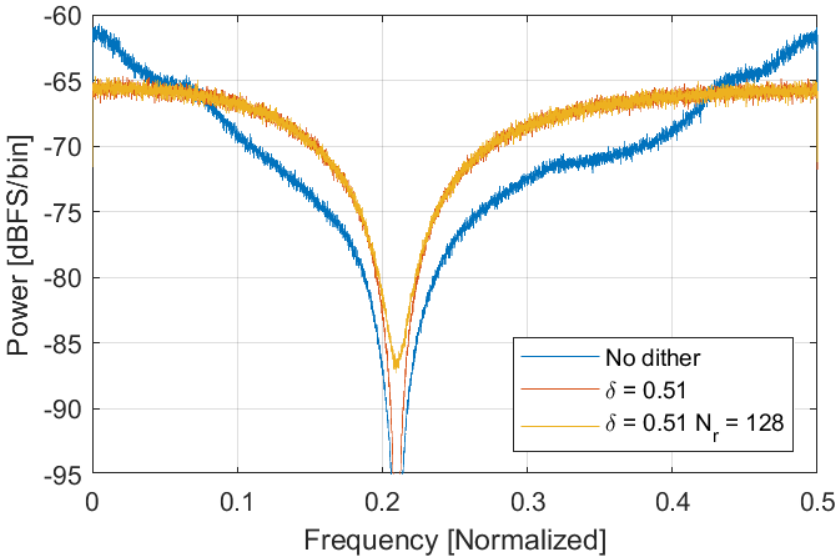

Figure 26: Typical tree DEM NSD, DSM sinusoid input

6 Noise Performance

The tone mitigation schemes presented add dither and therefore incur a noise penalty. This additional noise will be treated here. Noise contribution from coefficient quantization and round-off will be covered in the implementation section.

To start, in-band noise of a full 16 unit DAC DEM is shown in figure 27 at different over sampling ratios (OSR). This noise is a typical plot taken at a center frequency of 0.21 and does not vary substantially from these nominal values. The input under consideration is a fourth order bandpass DSM modulated sinusoid, with the center frequency matched with that of the DEM. As well, unit cell variance of 1 percent is assumed. The first scheme ($\delta = 0.51$) imposes a consistent 4 dB penalty overall. The additional noise is introduced near the quantizer and is shaped along with it.

First, adding a dither region (orange curve) adds a consistent 4 dB or so of in-band noise as compared to the no dither case (blue curve). This is consistent with previous observed noise spectral such as figure 26. Even at high OSRs, there is no indication of a noise floor. Dither-and-reset, however, behaves differently.

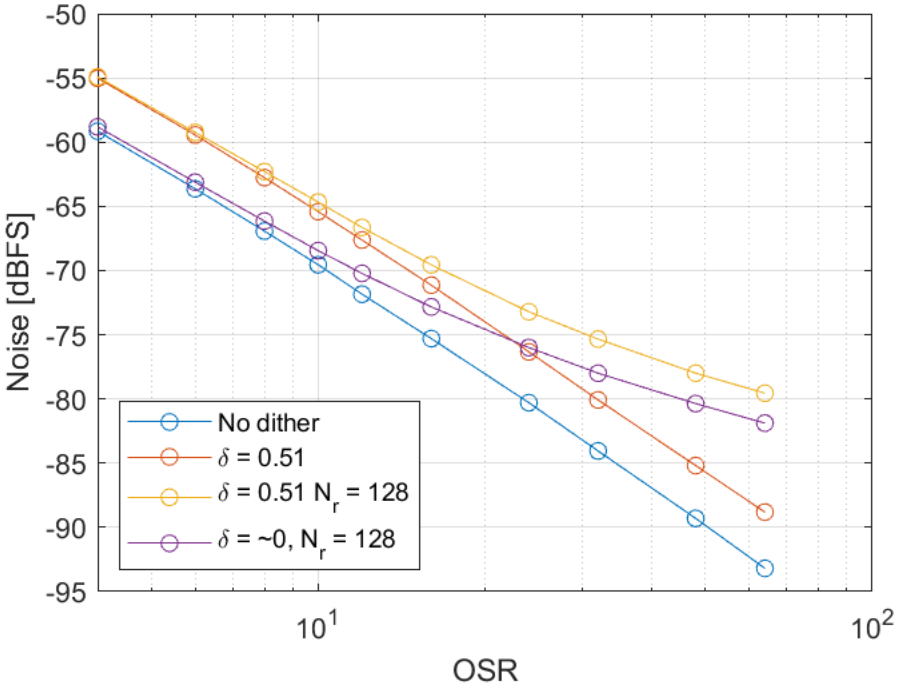

Figure 27: In-band noise over OSR

Dither-and-reset exhibits a noise floor. This noise floor is evident from the yellow curve in figure 27. Even if the dither region is shrunk to almost zero (curve: $\delta =\sim 0$, $N_r = 128$) the noise floor is still observed. To explain this behaviour, a rough noise floor estimate is established. First, consider reset events as a subtraction of the resonator from itself. The resonator value at reset is then separated from the rest of the loop by way of an additional noise source. This noise is $q_r[n]$ and $q_i[n]$ of figure 28.

From this model, noise can be estimated. As the integrator is uncorrelated from one reset to the next, from theorem 3, $q[n]$ will be as well. Even further, $q[n]$ is only non-zero at resets and therefore its real and imaginary components can be modelled as white noise. It is as if a specially designed dither is added directly to the resonator instead of the quantizer. Recognizing that the path from both the real and imaginary portions of $q[n]$ to $s[n]$ form the signal path of a DSM, its transfer function has unity gain at f_c. At this juncture, a number of assumptions are made. First, the real and imaginary components of $q[n]$ are

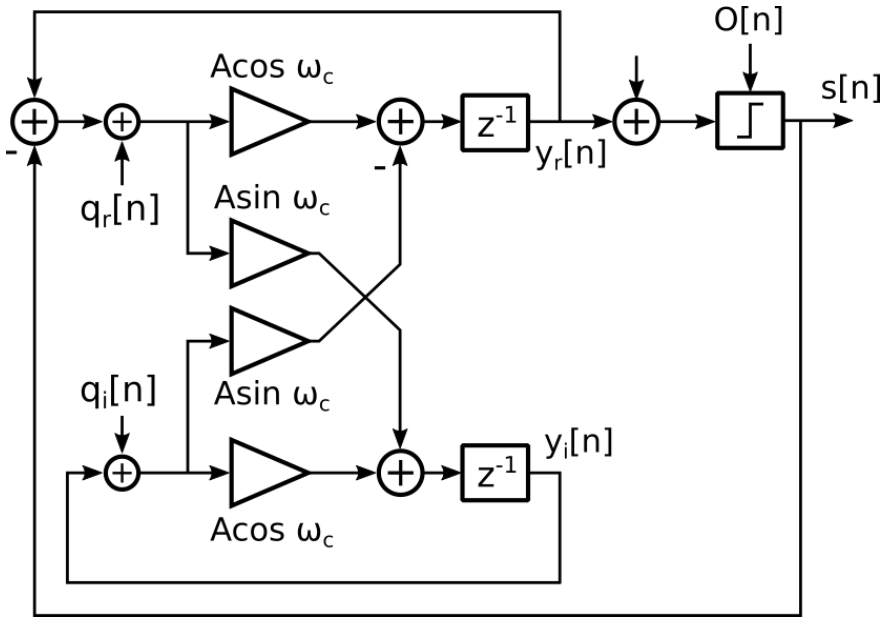

Figure 28: Reset noise model

uncorrelated. Second, $d_2[n]$ is uncorrelated with the quantizer noise. And thirdly, $x[n]$ is only odd. Combining all above assumptions, a noise floor is confirmed as the equivalent white noise injected at $q[n]$ directly goes to the output un-shaped. Also, a loose estimate of its variance becomes equation (10)

$$\sigma^2_{reset} = \frac{E\{|s[n]|^2\}}{N_r} \tag{10}$$

, where $E\{|s[n]|^2\}$ is approximately 1 for most inputs and f_c. First, this estimates confirms that the noise floor is inversely proportional N_r. At high OSR where this noise floor dominates, figure 29 agrees with this result: as Nr decreases from 256 to 64, the in-band noise increases by 6 dB. As well, this estimate predicts the in-band noise with Nr = 128 to be the green curve in figure 29 which is approximately 3 dB off from the yellow curve. Lastly, this noise floor varies only lightly with most input waveforms indicating the third assumption ($x[n]$ being only odd) may not be entirely needed.

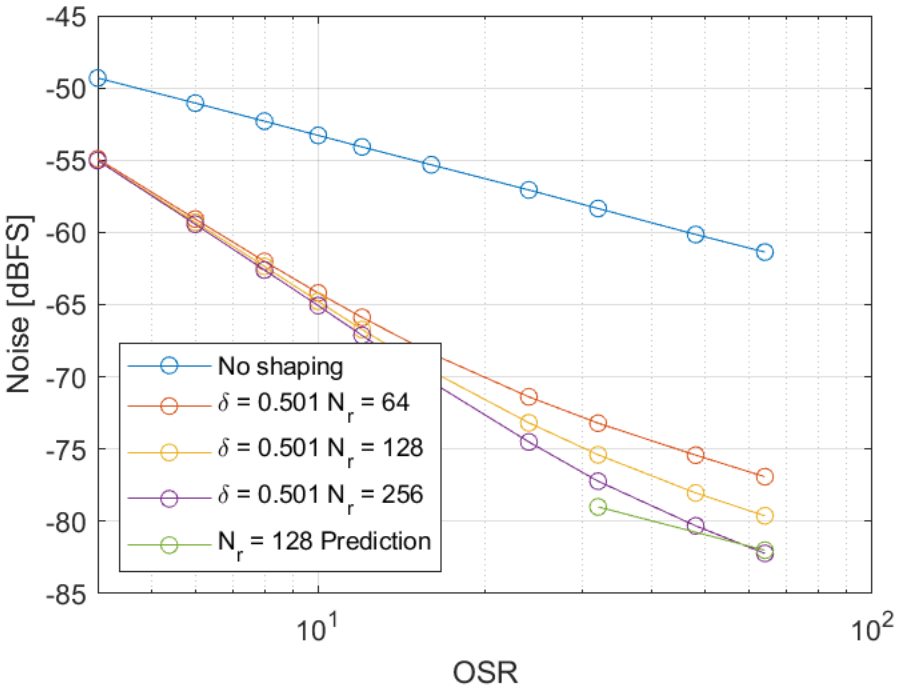

Figure 29: In-band noise over Nr

7 Implementation

Multiple implementation aspects require consideration. First, a design example will treat aspects under design control: coefficient quantization, multiplier round-off and reset period. DEM hardware complexity and speed for said design are covered afterwards. The requirements for this example will be an in-band noise suppression requirement of 10 dB at an OSR of 16.

7.1 Hardware Design

Quantizer noise notwithstanding, the primary noise contributor stems from coefficient quantization, the coefficients being $\cos\omega_c$ and $\sin\omega_c$. Coefficient quantization leads to an error in f_c and A, as per 12. Three example resolutions are shown in figure 30. As the resolution changes from 10 fractional bits to 5 and then 3, the center frequency moves off band and the

noise trough degrades. To address the change in f_c, this design example will limit its error to roughly 10 % of the in-band bandwidth. As such, 5 fractional bits are required for both coefficients. For the integer portion, $Re\{y[n]\}$ and $Im\{y[n]\}$ rarely exceeds a magnitude of 4 and therefore 2 bits are allocated. This leads to a total of 6 bits plus a sign bit. As for the error in A, finite noise rejection at f_c occurs as evidenced by the modified transfer function (11). If adequate rejection is not achieved, design can instead start from limits imposed on A.

$$|S(e^{j\omega})|^2 = |Y(e^{j\omega})|^2(1 + A^2 - 2A\cos(\omega - \omega_c)) \tag{11}$$

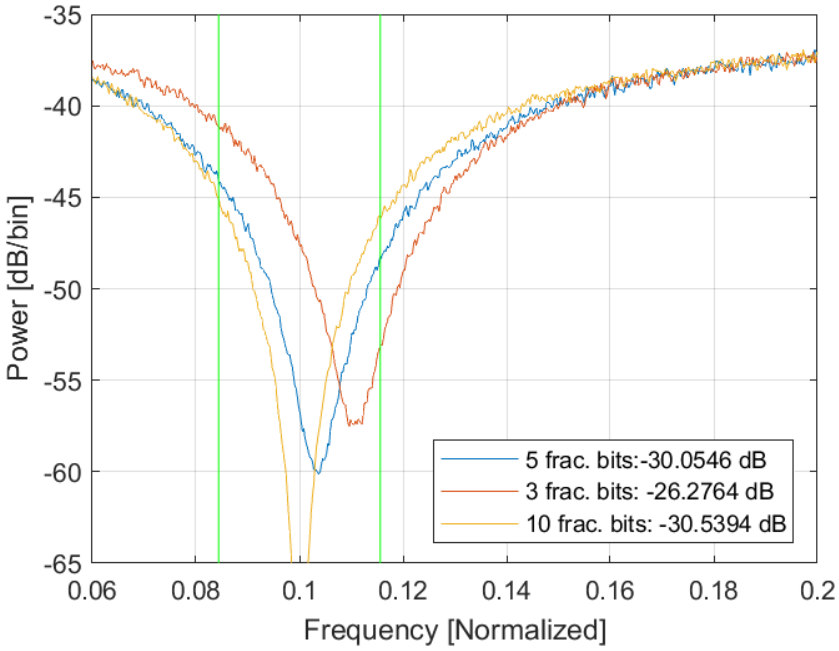

Figure 30: Effect of coefficient quantization

Multiplier round-off error raises concerns as well, foremost being tones. For the first strategy, dither region luckily does not need adjustment. When an odd input arrives, precisely ± 1 will still be subtracted from the resonator. In fact, with multiplier round-off, the dither region will effectively widen as a narrow strip slightly outside the dither region will

now be included. Considering this, a dither region slightly larger than $\delta = 0.5$ can be easily implemented by checking if all MSbs are 0 (or 1 if negative). With periodic resets, the lack of tones is preserved as long as the rounding is done symmetrically. The in-band noise penalty due to round-off error is minimal compared to shifts in f_c and A. Finally, quantization of $\cos\omega_c$ and $\sin\omega_c$ can lead to a A larger than 1. As such, these coefficients should be selected to place $A < 1$, especially if periodic reset is not employed.

The final step is the selection of N_r. Unfortunately, equation 10 was optimistic and after some simulation, N_r was set to 64. As for the implementation, resets are done on all layers synchronously. However, staggered resets are possible as well. The $s[n]$ PSD at various stages of design is shown in figure 31. With quantization and reset, the required in-band noise is achieved. Notice the shift in f_c and finite noise floor due to coefficient quantization alone. Resonator reset raises the floor further in the final step. The full tree DEM has a similar noise profile.

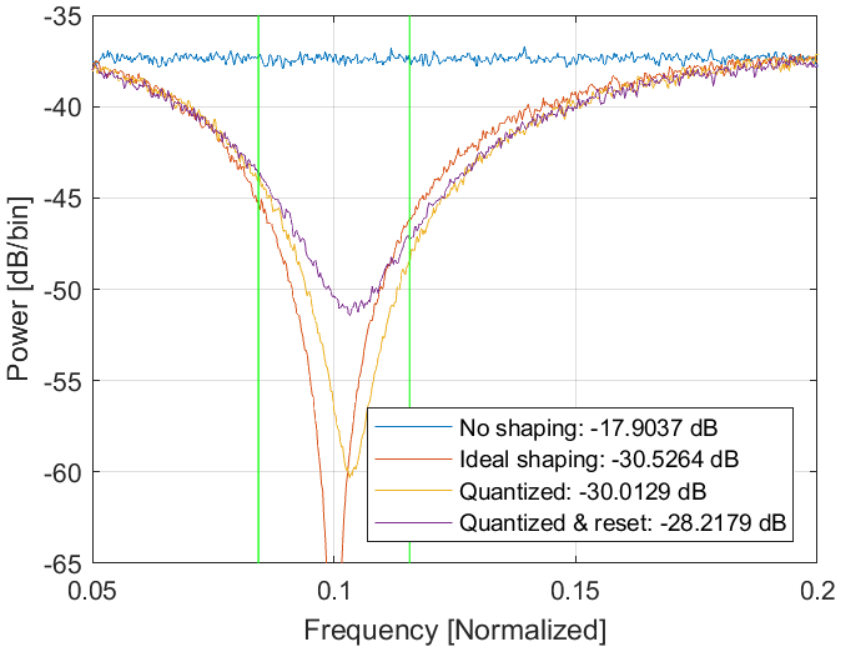

Figure 31: Design example

7.2 Complexity and Speed

Ensuring the absence of tones does incur hardware overhead and is broken down in table 3. The dither region requires a magnitude comparator for each switching block and a PRBS generator. The PRBS generator can be shared amongst all s-blocks within a layer. From simulation, sharing the random sequence negligibly effects noise. Without justification, a 23-bit linear file shift register is assumed and imposes the majority of the additional hardware required. It can be optimized for a particular tone performance. As for the resonator reset, only a 6 bit synchronous counter is required for the entire tree. The gate estimates for this single s-block are independent of DAC resolution.

Comparator (Per s-block)	PRBS Generator (Per layer)	Reset Counter (Per DEM)	Rest of s-block (Per s-block)
11	170	70	1100

Table 3: Estimated s-block gate count

As for speed, one of two possible critical paths can limit speed: the switching network and the $y_r[n+1]$ calculation. The band-pass sequence generator's additional complexity can add delay to the switching network depending on how the magnitude comparison is performed. If the comparison is place as per the dither in 12, the $s[n]$ computation in the first s-block would add a fixed 4 gate delay to the entire tree. Alternatively, the comparison can be performed off of $y[n+1]$ and latched. This second approach removes the delay at the expense of an additional flip-flop.

The second possible critical path is in the $y_r[n+1]$ calculation. It consists of the switching and parity networks, the comparison and the add-multiply-add operations. This path will most likely place the upper limit on the DEM speed.

7.3 Scheme Summary

A summary of the schemes discussed is written here. The hardware breakdown of the entire tree due to the toneless criteria is presented first. Assuming a high-speed switching network from [8], the gate count required for the entire 4-bit DAC DEM is summarized in table 4. Imposing toneless behaviour adds minimal hardware on band-pass DEM. Overall, band-pass DEM does require substantial hardware compared to low-pass DEM due to the four multipliers. Alternate filter structures that both have fewer multipliers and can preserve PMF symmetry of theorem 2 have not been investigated.

Hardware	Low-pass DEM	Band-pass DEM
Toneless requirement overhead	690	880
Rest of DEM	330	16000

Table 4: Estimated gate count of 4-bit low-pass and band-pass DEM

A broader summary of existing tunable band-pass DEM are shown in table 5 and schemes presented herein are shown in table 6. Unless superseded by a note, hardware is measured in the number of 2 in gates. As well, note shaping is the noise improvement over DEM with no shaping at all. As each scheme has different design criteria and special cases so a few notes are added in parenthesis.

	[11] (analog)	[16]
Hardware	1645 (1)	16000 (2)
Levels	8	16 (2)
Noise shaping [dB]	20 (3)	10 (OSR = 16)(2)
Toneless	Unclear	No
Features	None	I/Q DEM

Table 5: Summary of choice existing tunable BPDEM

Note (1): this is the number of transistors. Note (2): this is this author's own estimate based on the above design example. Note (3): no OSR is explicitly designed for. Note (4): assuming 8 integrators which would correspond to tuning down to 1/8.

	Dither and reset DEM	DSM N-path DEM
Hardware	17000	1900 (4)
levels	16	16
Noise shaping [dB]	10 (OSR = 16)	6 (OSR = 16)
Toneless	Yes	Yes
Features	None	None

Table 6: Summary of new tunable BPDEM

8 Future Work

With toneless operation guaranteed, this work can be expanded upon on multiple fronts. The first of which is to simplify the existing structure. The toneless property was proven for a state-space implementation. If proven for a direct form 2, such structure would cut down on multipliers by half and substantially simplify the required hardware. It should be noted that the critical paths would remain the same.

The structure presented can also be extended to 4th order band-pass shaping similar to the 2nd order high-pass shaping in [8]. A proposed implementation is shown in figure 32. A second resonator would serve the purpose of the second integrator in [8]. The quantizer would first check if $|Re\{y_1[n]\}| \leq \delta$ and if true, would check $y_2[n]$. The dither region would be applied on $y_2[n]$ instead. Preliminary simulations indicate the absence of tones, as shown in figure 33. However, toneless behaviour has not been proven.

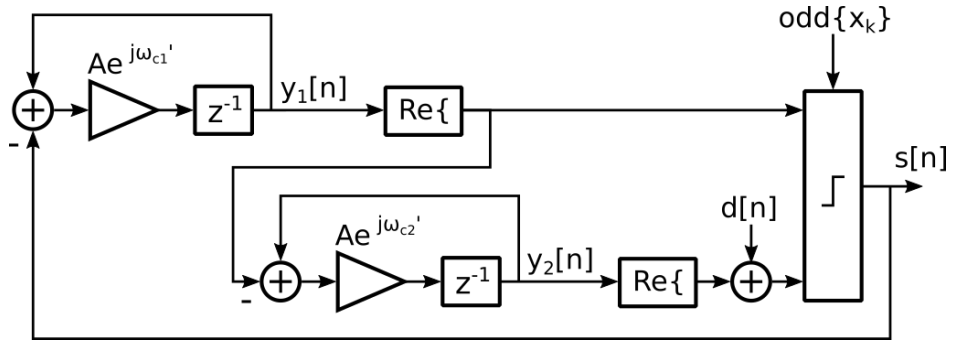

Figure 32: 4th order band-pass DEM

Finally, periodic reset can equally apply to vector-based shaping. Currently, only dither

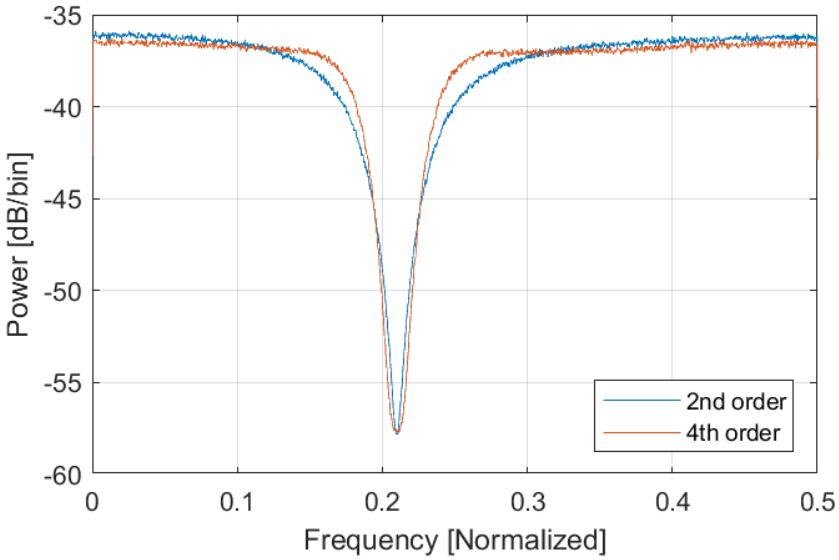

Figure 33: 4th order band-pass DEM

is typically applied. Additionally, internal states of each DSM would also be periodically reset and initialized to random states. It is not clear how dither should be applied. However, if for every selection sequence, there is an equally likely sequence which would produce the opposite error, tones may be dispersed entirely.

9 Conclusion

Much literature has been devoted to noise shaping techniques in DEM; however, on the subject of tones, no progress has been reported beyond first order shaping. Two strategies are proposed to address this. The first is the formation of dither region within which randomness is introduced. Although, absence of tones is not guaranteed, tonal behaviour is rare. The second strategy builds on top of the first and resets the resonator. Combined, they become provably toneless. A noise penalty is incurred but it can be partially controlled. As well, although the hardware required is large, the overhead imposed to guarantee the absence tones is relatively minor.

10 Appendix A: Proofs

The appendix provides the supporting proofs for both DSM N-path DEM and reset-and-dither DEM. Theorem 1 shows the toneless property of the first scheme. The rest of the theorems, culminating in theorem 4, show the toneless property of the second scheme.

Theorem 1. *Given any sequence $O[n]$ and path selection pattern, the N-path sequence generator generates a sequence $s[n]$ which is toneless.*

Proof. The single path s-block is known to be toneless as per [9]. The DSM N-path s-blocks can be decomposed into N traditional s-blocks, each of which generates separate toneless sequences. Therefore, it is only necessary to prove that interleaving these sequences into the intended sequence is toneless.

Two sequences $x[n]$ and $y[n]$ are toneless if their PSDs are bounded:

$$S_{xx}(e^{j\omega}) = \lim_{N\to\infty} \frac{1}{N} E\left\{ \left| \sum_{n=0}^{N-1} x[n] e^{-j\omega n} \right|^2 \right\} < C_x < \infty \forall \omega \tag{12}$$

$$S_{yy}(e^{j\omega}) = \lim_{N\to\infty} \frac{1}{N} E\left\{ \left| \sum_{n=0}^{N-1} y[n] e^{-j\omega n} \right|^2 \right\} < C_y < \infty \forall \omega \tag{13}$$

Which, for the ease of recognition, can be rewritten as the following:

$$S_{xx}(e^{j\omega}) = \lim_{N\to\infty} \frac{1}{N} \sum_{n=0}^{N-1} \sum_{m=0}^{N-1} E\left\{ x[n]x[m]e^{-j\omega n} e^{j\omega m} \right\} \tag{14}$$

$$S_{yy}(e^{j\omega}) = \lim_{N\to\infty} \frac{1}{N} \sum_{n=0}^{N-1} \sum_{m=0}^{N-1} E\left\{ y[n]y[m]e^{-j\omega n} e^{j\omega m} \right\} \tag{15}$$

These sequences must then be combined to create the intended sequence. To this end, interleaving would expand and shift the sequences, creating two new sequences, $x_2[n]$ and $y_2[n]$. They themselves would have bounded PSDs as expansion simply compresses the

spectrum and time shifts have no effect on the spectrum magnitude. Summing these two sequences creates a new sequence, $z[n]$, and taking its PSD yields:

$$S_{zz}(e^{j\omega}) = \lim_{N\to\infty} \frac{1}{N} E\left\{ \left| \sum_{n=0}^{N-1} x_2[n]e^{-j\omega n} + y_2[n]e^{-j\omega n} \right|^2 \right\} \tag{16}$$

$$\begin{aligned} S_{zz}(e^{j\omega}) = \lim_{N\to\infty} \frac{1}{N} \sum_{n=0}^{N-1}\sum_{m=0}^{N-1} (&E\{x_2[n]x_2[m]\} + E\{y_2[n]x_2[m]\} \\ &+E\{x_2[n]y_2[m]\} + E\{y_2[n]y_2[m]\})e^{-j\omega n}e^{-j\omega m} \end{aligned} \tag{17}$$

However, $E\{x_2[n]y_2[m]\} = 0 \forall m, n$ because, their choice of ± 1 (if not zero) is independent even though the sequences are related through $odd\{x_{k,n}\}$. Without the cross-terms, the PSD of z[n] is itself composed of finite bounded PSDs $S_{x_2x_2}(e^{j\omega})$ and $S_{y_2y_2}(e^{j\omega})$ which indicates $z[n]$ is toneless.

□

Theorem 2. *The marginal PMFs of $Re\{Y[n]\}$ and $Im\{Y[n]\}$ for every n generated by the iterative function*

$$y[n+1] = A(y[n] - s[n])e^{j\omega_c} \tag{18}$$

where

$$s[n] = \begin{cases} 0, & O[n] = 0 \\ sign\{Re\{y[n]\}\}, & O[n] = 1 \text{ and } |Re\{y[n]\}| \leq \delta \\ d[n], & otherwise \end{cases}$$

are symmetric for any given $O[n]$.

Proof. For the sake of notation, the random variables $Re\{Y[n]\}$ and $Im\{Y[n]\}$ will be abbreviated as $Y_{r,n}$ and $Y_{i,n}$, respectively. The marginal PMFs of $Y_{r,n}$ and $Y_{i,n}$ are symmetric

if

$$\begin{aligned} P_{Y_{r,n}}(r_n) &= P_{Y_{r,n}}(-r_n) \forall r_n \\ P_{Y_{i,n}}(i_n) &= P_{Y_{i,n}}(-i_n) \forall i_n. \end{aligned} \tag{19}$$

The proof will proceed in two steps: first, symmetry in the joint PMF $P_{Y_{r,n},Y_{i,n}}(r_n, i_n)$ is linked to the marginal PMFs and then joint PMF symmetry is proven over all n.

For the first step, the PMF of $Y_{r,n}$ is derived as follows. If the joint PMF is symmetric, i.e.

$$P_{Y_{r,n},Y_{i,n}}(r_n, i_n) = P_{Y_{r,n},Y_{i,n}}(-r_n, -i_n) \forall r_n, i_n, \tag{20}$$

then it follows that

$$P_{Y_{r,n}}(-r_n) = \sum_{i_n} P_{Y_{r,n},Y_{i,n}}(-r_n, i_n) \tag{21}$$

$$= \sum_{-i_n} P_{Y_{r,n},Y_{i,n}}(-r_n, -i_n) \tag{22}$$

$$P_{Y_{r,n}}(-r_n) = P_{Y_{r,n}}(r_n) \forall r_n. \tag{23}$$

A similar argument can be made to show

$$P_{Y_{i,n}}(-i_n) = P_{Y_{i,n}}(i_n) \forall i_n, \tag{24}$$

which completes the first portion of the proof.

For the second portion of the proof, it is to be shown that (20) is true for any n. A proof by induction follows. For the base case, equation (20) is satisfied when $Y[n]$ is reset: only one value is likely and it is at 0. For the induction step, for any subsequent n, (20) can be broken up into an odd and even cases as $O[n]$ is given. For notational simplicity, the conditions on $O[n]$ are dropped and the substitutions for the constants $A \sin \omega_c = A_s$ and $A \cos \omega_c = A_c$ are made.

Case 1) Even case ($O[n] = 0$):

If (20) is true then applying the iterative function, it is evident that

$$P_{Y_{r,n+1},Y_{i,n+1}}(r_{n+1}, i_{n+1}) = P_{Y_{r,n+1},Y_{i,n+1}}(-r_{n+1}, -i_{n+1}) \forall r_{n+1}, i_{n+1} \tag{25}$$

Case 2) Odd case ($O[n] = 1$):

The odd case is not as straightforward as the iterative function must be expanded; the expressions are written out on separate lines. The joint PMF $P_{Y_{r,n},Y_{i,n}}(r_n, i_n)$ is decomposed into the sum of conditional PMFs:

$$Pr(C) P_{Y_{r,n},Y_{i,n}}(r_n, i_n|C) \tag{26}$$

$$Pr(C^*) P_{Y_{r,n},Y_{i,n}}(r_n, i_n|C^*) \tag{27}$$

Where C and C^* are equally likely events such that $Y_{r,n} > \delta \vee (|Y_{r,n}| < \delta \wedge d[n] = 1)$ and $Y_{r,n} < -\delta \vee (|Y_{r,n}| < \delta \wedge d[n] = -1$, respectively. Applying the iterative function, at $n + 1$, the terms above become

$$Pr(C) P_{Y_{r,n+1},Y_{i,n+1}}((r_n - 1)A_c - i_n A_s, (r_n - 1)A_s + i_n A_c|C) \tag{28}$$

$$Pr(C^*) P_{Y_{r,n},Y_{i,n}}((r_n + 1)A_c - i_n A_s, (r_n + 1)A_s + i_n A_c|C^*) \tag{29}$$

Similarly, the joint PMF $P_{Y_{r,n},Y_{i,n}}(-r_n, -i_n)$ is composed of the conditional probabilities and with some manipulation yields

$$Pr(C^*) P_{Y_{r,n+1},Y_{i,n+1}}((-r_n - 1)A_c + i_n A_s, (-r_n - 1)A_s - i_n A_c|C^*) \tag{30}$$

$$Pr(C)P_{Y_{r,n+1},Y_{i,n+1}}((-r_n+1)A_c+i_nA_s,(-r_n+1)A_s-i_nA_c|C) \tag{31}$$

Rearranging signs of (30) and (31) yields

$$Pr(C^*)P_{Y_{r,n+1},Y_{i,n+1}}(-((r_n+1)A_c-i_nA_s),-(r_n+1)A_s+i_nA_c)|C^*) \tag{32}$$

$$Pr(C)P_{Y_{r,n+1},Y_{i,n+1}}(-((r_n-1)A_c-i_nA_s),-((r_n-1)A_s+i_nA_c)|C). \tag{33}$$

Noticing that the terms (28), (29) are negatives of (33), (32), respectively, it must be that

$$P_{Y_{r,n+1},Y_{i,n+1}}(r_{n+1},i_{n+1})=P_{Y_{r,n+1},Y_{i,n+1}}(-r_{n+1},-i_{n+1})\forall r_{n+1},i_{n+1}. \tag{34}$$

By induction, equation (20) is satisfied for all n. Combining the results from both portions of this proof, it must be that the marginal PMFs of $Re\{Y[n]\}$ and $Im\{Y[n]\}$ are symmetric for all n. □

Lemma 1. *Given any sequence $O[n]$, the expectation $E\{y[n]\}=0$ for the update function* (18).

Proof. Expanding the expectation reveals the two random variables, $Re\{Y[n]\}$ and $Im\{Y[n]\}$, which have symmetric PMFs as per theorem 2. As a random variable with a symmetric PMF would have an expectation of zero, the lemma follows from this fact. □

Theorem 3. *The expectation $E\{y[m]y^*[n]\}=0\forall m,n \ni m<N_r\leq n$ if $y[N_r]=0$, given any sequence $O[k]\forall k$ for the update function* (18).

Proof. The random variables $Y[m]$, $Y[n]$ are not independent for $m<N_r\leq n$ because of $O[k]$; however, conditioned on any sequence $O[k]$ for $N_r\leq k\leq n$, independence is assured

due to the intervening reset. Expanding out the expectation

$$\begin{aligned} E\{y[m]y^*[n]\} &= \sum_{O_{i,k}\in\{O[k]\ni N_r\le k\le n\}} Pr\{O_{i,k}\}E\{y[m]y^*[n]|O_{i,k}\} \\ &= \sum_{O_{i,k}\in\{O[k]\ni N_r\le k\le n\}} Pr\{O_{i,k}\}E\{y[m]\}E\{y^*[n]|O_{i,k}\}. \end{aligned}$$

From lemma 1, all $E\{y^*[n]|O_{i,k}\}$ above are zero; therefore, the theorem holds. □

Theorem 4. *Given a sequence $O[n]$, the sequence generator with the iterative function*

$$y[n+1] = A(y[n] - s[n])e^{j\omega_c} \tag{35}$$

where

$$s[n] = \begin{cases} 0, & O[n] = 0 \\ sign\{Re\{y[n]\}\}, & O[n] = 1 \text{ and } |Re\{y[n]\}| \le \delta \\ d[n], & otherwise \end{cases}$$

is toneless if integrator resets occur at most with finite intervals N_r.

Proof. The expected periodogram can be expanded and rewritten as a summation of autocorrelation terms. The proof will focus on this autocorrelation.

$$E\{P_N(e^{j\omega})\} = \frac{1}{N}\sum_{m=0}^{N-1}\sum_{n=0}^{N-1} E\{y[m]y^*[n]\}e^{-j\omega(n-m)} \tag{36}$$

As shown in Theorem 3, $y[n]$ is uncorrelated across resets. This allows equation (36) to be broken down; the analysis proceeds similarly to [9]. $y[n]$ can be expressed as a series of symbols where resets mark the leading sample,

$$y[n] = \sum_{k=0}^{\infty} y[n]w_k[n], \tag{37}$$

where the windowing sequence $w_k[n]$ is 1 only for the kth symbol. In contrast, high pass shaping marks symbols at every second ± 1 sample in the $s[n]$ sequence.

Substituting equation (37) into (36) becomes

$$E\{P_N(e^{j\omega})\} = \frac{1}{N} \sum_{m=0}^{N-1} \sum_{n=0}^{N-1} \sum_{k=0}^{N_{sym}-1} \sum_{l=0}^{N_{sym}-1} E\left\{y[m]y^*[n]w_k[m]w_l[n]\right\} e^{-j\omega(n-m)} \tag{38}$$

where N_{sym} is the number of symbols which constitute the first N samples. Noting that symbols are uncorrelated across symbols (i.e. the expectation is only non-zero if $k = l$), consolidation of terms yields

$$E\{P_N(e^{j\omega})\} = \sum_{k=0}^{N_{sym}-1} E\left\{ \frac{1}{N} \left| \sum_{n=0}^{N-1} y[n]w_k[n]e^{-j\omega n} \right|^2 \right\}. \tag{39}$$

Each symbol is at most length N_r, therefore (39) has a magnitude of at most $\frac{N_r^2 N_{sym}}{N}$. As $N_{sym} \propto N$ (or $N_{sym} = \frac{N}{N_r}$ if all symbols are length N_r), the limit of (39) is finite as $N \to \infty$.

□

References

[1] R. Van de Plassche and D. Goedhart, "A monolithic 14-bit d/a converter," *IEEE Journal of Solid-State Circuits*, vol. 14, no. 3, pp. 552–556, 1979.

[2] L. Carley, "A noise-shaping coder topology for 15+ bit converters," *IEEE Journal of Solid-State Circuits*, vol. 24, no. 2, pp. 267–273, 1989.

[3] R. Baird and T. Fiez, "Improved /spl delta//spl sigma/ dac linearity using data weighted averaging," in *Proceedings of ISCAS'95 - International Symposium on Circuits and Systems*, vol. 1, 1995, pp. 13–16 vol.1.

[4] R. Schreier and B. Zhang, "Noise-shaped multbit d/a convertor employing unit elements," *Electronics Letters*, vol. 31, no. 20, pp. 1712–1713, 1995.

[5] S. Pavan, R. Schreier, and G. C. Temes, *Understanding Delta-Sigma Data Converters 2nd Ed*, 2017.

[6] I. Galton, "Spectral shaping of circuit errors in digital-to-analog converters," *IEEE Transactions on Circuits and Systems II: Analog and Digital Signal Processing*, vol. 44, no. 10, pp. 808–817, 1997.

[7] J. Welz and I. Galton, "Necessary and sufficient conditions for mismatch shaping in a general class of multibit dacs," *IEEE Transactions on Circuits and Systems II: Analog and Digital Signal Processing*, vol. 49, no. 12, pp. 748–759, 2002.

[8] J. Welz, I. Galton, and E. Fogleman, "Simplified logic for first-order and second-order mismatch-shaping digital-to-analog converters," *IEEE Transactions on Circuits and Systems II: Analog and Digital Signal Processing*, vol. 48, no. 11, pp. 1014–1027, 2001.

[9] J. Welz and I. Galton, "The mismatch-noise psd from a tree-structured dac in a second-order delta sigma modulator with a midscale input," vol. 4, 02 2001, pp. 2625 – 2628 vol.4.

[10] R. Schreier and B. Zhang, "Noise-shaped multbit d/a convertor employing unit elements," *Electronics Letters*, vol. 31, pp. 1712–1713(1), September 1995.

[11] T. S. Kaplan, J. F. Jensen, C. H. Fields, and M. . F. Chang, "A 2-gs/s 3-bit delta sigma-modulated dac with tunable bandpass mismatch shaping," *IEEE Journal of Solid-State Circuits*, vol. 40, no. 3, pp. 603–610, 2005.

[12] T. Ueno, A. Yasuda, T. Yamaji, and T. Itakura, "A fourth-order bandpass delta-sigma modulator using second-order bandpass noise-shaping dynamic element matching," *IEEE Journal of Solid-State Circuits*, vol. 37, no. 7, pp. 809–816, 2002.

[13] T. Shui, R. Schreier, and F. Hudson, "Mismatch shaping for a current-mode multibit delta-sigma dac," *IEEE Journal of Solid-State Circuits*, vol. 34, no. 3, pp. 331–338, 1999.

[14] W. Akram and E. E. Swartzlander, "Tunable mismatch shaping for quadrature bandpass delta-sigma data converters," in *2010 IEEE Workshop On Signal Processing Systems*, 2010, pp. 198–203.

[15] V. O'Brien and B. Mullane, "High order mismatch shaping for low oversampling rates," *IEEE Transactions on Circuits and Systems II: Express Briefs*, vol. 67, no. 1, pp. 42–46, 2020.

[16] Song-Bok Kim, S. Joeres, R. Wunderlich, and S. Heinen, "Complex mismatch shaper for tree-structured dac in multi-bit complex sigma-delta modulators," in *2008 15th IEEE International Conference on Electronics, Circuits and Systems*, 2008, pp. 328–331.

[17] S. Lindfors, P. Ööpik, and K. Halonen, "N-path dynamic element maching for multi-bit bandpass sigma delta modulators," *International Journal of Circuit Theory and Applications*, vol. 25, pp. 335–346, 09 1997.

[18] J. Welz and I. Galton, "A tight signal-band power bound on mismatch noise in a mismatch-shaping digital-to-analog converter," *Information Theory, IEEE Transactions on*, vol. 50, pp. 593 – 607, 05 2004.

[19] W. Akram and E. Jr, "Tunable n-path mismatch shaping for multibit bandpass delta-sigma modulators," 12 2009, pp. 1288 – 1291.